Chapter

Plasmonic Interaction in Enhanced Luminescent Down-Shifting Layers for Photovoltaic Devices

***H. Ahmed*[a] *A. Sethi*[a] *J. Doran*[b] *and S. J. McCormack*[a]**

a School of Engineering, Trinity College Dublin, Dublin, Ireland.
b Dublin Energy Lab, Dublin Institute of Technology, Dublin, Ireland.

ABSTRACT

Harvesting solar energy has the potential to reduce carbon emissions and to provide clean energy contributing to sustainable development. Most photovoltaic (PV) research to date has focused on achieving higher PV conversion efficiency at lower cost. However, spectral losses due to limited spectral response of solar cells represent a fundamental limit to the maximum efficiency achievable by the single p-n junction solar cells. Low energy photons are not absorbed by the solar cell, while high energy photons are not used efficiently and energy is lost via thermalization. The potential exists to increase the solar cell efficiency by making better use of short wavelength light. One way to do this is to use a luminescent material to convert high energy photons to lower energy photons before the interaction with the solar cells occurs, a process referred to as luminescent down shifting (LDS). LDS suffers from self-absorption which undermines the efficiency of the LDS device. The downshifted photons are re-absorbed by the material within the down shifting layer which is a function of optical path length, concentration, and Stokes shift.

A novel approach was proposed to utilize metal nanoparticles with the objective of counteracting these optical loss mechanisms (Ahmed, 2015, Ahmed, et al., 2016a). Plasmonic Luminescent Down-Shifting (pLDS) is a new optical approach to increase a PV device efficiency by using plasmonic coupling between luminescent materials and metal nanoparticles (MNP). The optical properties of fluorescent species can exhibit dramatic spectral changes in the presence of metal nanoparticles. In this chapter, luminescent materials suitable for incorporation in LDS layers are described. A literature review on solar cell optical response and efficiencies is presented and plasmonic interaction of metal nanoparticles is discussed. Fabricated pLDS devices are presented along with their optical and electrical characterization. The results have shown significant enhancement in absorption, fluorescence emission and electrical output of the plasmonic photovoltaic devices

Keywords: Spectral losses; Photovoltaics; Luminescent materials; Plasmonic luminescent down-shifting layers

* Corresponding Author Email: hahmed@tcd.ie

INTRODUCTION

Photovoltaic (PV) technologies have developed rapidly since the 1950s and continue to do so due to concerns over finite conventional fossil fuel supplies and carbon emissions. The current world consumption of energy is 13 TW per year. By 2050, the annual world energy consumption is projected to be ~ 27.6 TW per year [Tsao et al., 2006]. Harvesting solar energy has the potential to reduce carbon emissions and to provide clean energy contributing to sustainable development.

In principle, PV cells convert incident sunlight directly into electricity by a process known as the photovoltaic effect [Becquerel, 1840, Angrist, 1982], whereby an electrical current is produced when sunlight is incident on certain semiconducting materials such as silicon (Si), and Gallium Arsenide (GaAs). When a photon is absorbed by such materials, its energy is given to tightly bound valence band electrons. Upon excitation, the valence band electron moves into the conduction band and leaves a positively charged hole in the valence band, provided that the energy of the incident photon is greater or equal to the energy gap of the solar cell material (for example, Si energy band gap is 1.1eV at room temperature).

Most of the photovoltaic research to date has focused on achieving higher photovoltaic conversion efficiency at lower cost. Cost, often expressed in terms of US $/W, remains one of the greatest barriers for PV to compete with and replace existing conventional energy resources.

The current PV market consists of a range of technologies which have been grouped from current first-generation, to second and third-generation technologies [Green, 2002; 2003; 2006, Zweibel, 2005, Bagnall & Boreland, 2008, Razykov et al., 2011, SunShot Vision Study, 2012, ETSAP and IRENA, 2013, Green et al., 2015]. Figure 1 shows the increase in laboratory best cell efficiencies of PV technology over the past few decades [NREL, 2016].

First-generation PVs are crystalline silicon or wafer based single-junction solar cells, including single crystalline (c-Si) and multi-crystalline silicon (mc-Si). Crystalline silicon technologies constitute about 85% of the current PV market [SunShot Vision Study, 2012, ETSAP and IRENA, 2013, EurObserv'ER, 2016]. The efficiency of the best current commercial c-Si PV modules has reached about 25.6 ± 0.5% [Green et al., 2015, NREL, 2016]. The average efficiency of the majority of the c-Si and mc-Si PV current commercial modules is 13-19% [SunShot Vision Study, 2012, ETSAP and IRENA, 2013, Green et al., 2015] and up to 27.6% for single crystalline concentrator Si cells [NREL, 2016] has been achieved in some labs as presented in figure 1.

Second-generation PV was developed using thin film technologies to remove unnecessary materials cost while maintaining efficiencies of first-generation PV. The second-generation PVs are single junction thin film devices utilizing amorphous-Si (a-Si), $Cu(In,Ga)Se_2$(CIGS), CdTe/CdS, or polycrystalline-Si (p-Si) deposited on low-cost substrates such as glass. Efficiencies of 21.3% for CdTe, and almost 23.3% for $Cu(In,Ga)Se_2$ as shown in figure 1 have been reported by leading laboratories for these thin film solar cells [NREL, 2016]. When scaling up to larger module sizes, an efficiency of 18.6±0.6% for CdTe, 12.3±0.3% for a-Si and 17.5±0.6% for CIGS modules have been reported [Green et al., 2015]. Therefore, the expansion of second-generation PV has been lower than originally expected for the technologies. Nevertheless, their potential remains to bring the cost of PV down in large scale production by reducing materials cost.

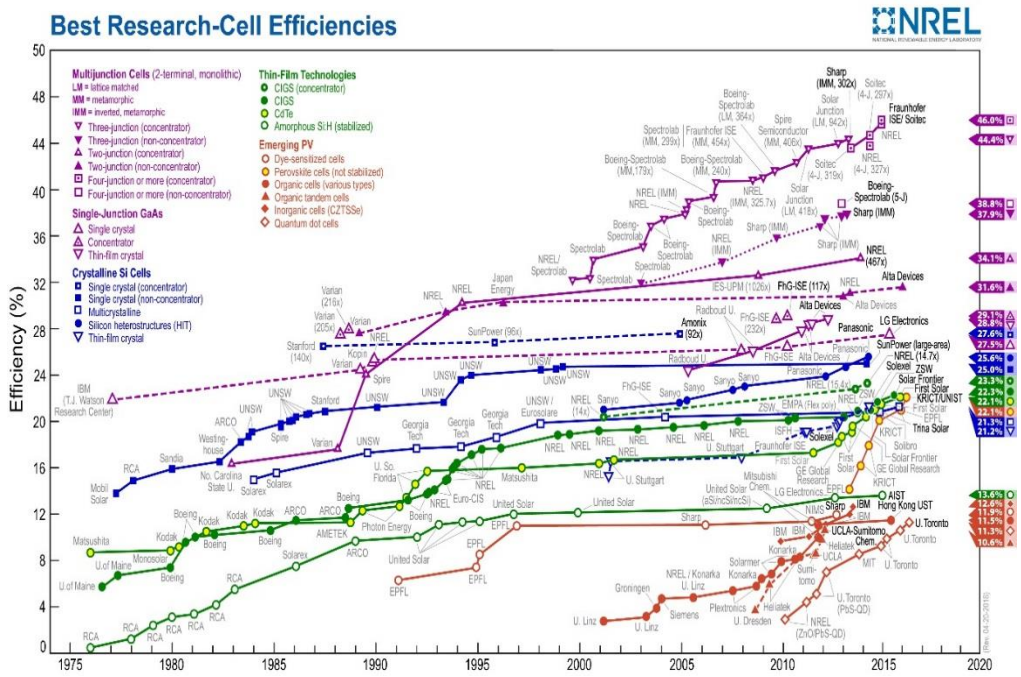

Figure 1: Evolution of the conversion efficiencies for various PV technologies and materials with their developers [NREL, 2016].

To maintain the cost reduction trend provided by second-generation PV, a higher efficiency is needed. This has led to the development of third-generation PV devices which exceed the limitation of single junction devices and lead to ultra-high efficiency, potentially for the same production cost of first and second PV generation [Green, 2006]. The development of third-generation PV is resulting in a more rapid increase in cell efficiency. For example, an efficiency of 30.4% in a double junction quantum well solar cell was demonstrated [Ekins-Daukes et al., 2009]. Also a maximum of 32% efficiency for thin film GaInP/GaAs/Ge triple-junction space PV [Karam et al., 1999] and 41.1 % for InGaP/InGaAs/Ge triple junction solar cell has been reported [Fraunhofer ISE, 2009]. The most recent improvements for triple - and four -junction solar cells lead to an increase in the efficiency to 44.4 % and 46.0 % respectively as can be seen in figure 1 [Fraunhofer ISE, 2016, NREL, 2016].

Continued development in PV technologies over the past few years has led to new device concepts such as dye-sensitised solar cells and organic solar cells [Benanti & Venkataraman, 2006, Wang, 2009]. The latter are based on polymers or small molecules with semiconductor properties [Boland et al., 2010] while dye-sensitised solar cells use dye molecules adsorbed onto a nanostructured substrate immersed in liquid or gel electrolyte to absorb solar radiation [Grätzel, M., 2003]. Dye-sensitised solar cells have demonstrated laboratory efficiencies as high as 11.1% and the organic solar cells have achieved efficiencies above 8%, see figure 1 [Razykov et al., 2011, SunShot Vision Study, 2012, NREL, 2016]. Their cost and efficiency however cannot compete with wafer based silicon devices at present, but the future development of these devices could result in revolutionary developments in photovoltaic technologies.

The cost of first-generation PV was reported in 2008 to be around US$4/W where half of this cost is due to 200-250µm thick silicon wafer. This thickness is required primarily for mechanical reasons since the majority of solar absorption occurs in the top ten microns of the cell [Green, 2006, Bagnall & Boreland, 2008]. The cost of mono- and multi-crystalline silicon modules in 2010, cited as low as $1.10/W [SunShot Vision Study, 2012]. However, this cost is not representative of all manufacturers and the typical prices ranged from $1.5/W-$2/W [Razykov et al., 2011, SunShot Vision Study, 2012]. Louwen et al., 2016 have recently analysed the production costs for silicon heterojunction (SHJ) solar cells compared them to conventional monocrystalline silicon modules. For their studied designs, module costs were calculated to be $0.48–0.56 per Watt-peak for SHJ modules, compared to $0.50 per Watt-peak for a conventional c-Si modules.

The cost of thin films PV modules has reached $0.64 in 2012 and has dropped to $0.53/W in 2013 [EurObserv'ER, 2014].

The cost of second-generation PV is also following the same trend. For example; the production cost in CdTe modules is presently around $0.72/W [SunShot Vision Study, 2012]. Generally, the cost per watt of the PV solar cells have been coming to decrease yearly. The average panel price worldwide has decreased from €0.63/W in 2013 to €0.52/W in 2015 [EurObserv'ER, 2016]. Figure 2 shows module price declines between 1976 and 2010 from $60/W to $2/W which indicate significant decrease on the PV solar cells prices over the years.

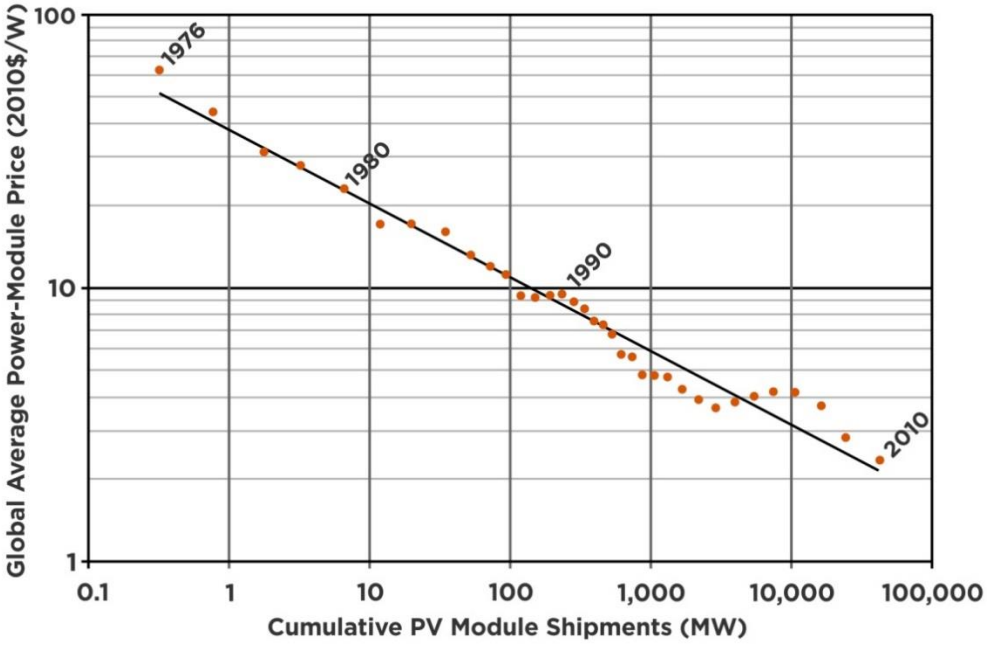

Figure 2: Decreasing PV module prices with cumulative sales [Drury et al., 2012].

In order for high efficiencies to be achieved in PV technologies, energy loss mechanisms must be reduced. One principle energy loss in the conversion of solar energy to electricity is

related to spectral losses, whereby low energy photons are not absorbed by the solar cell while high energy photons are not used efficiently.

The major loss mechanisms at short wavelengths are summarised below for various PV technologies [Klampaftis et al., 2009] in table 1.

Table 1: Major Optical Loss in PV Solar Cells

PV Solar cells	Major Optical Loss
Monocrystalline silicon (c-Si)	Emitter recombination, increased reflectance and absorption from anti- reflection coating (ARC).
Multi-crystalline silicon (mc-Si)	Recombination at the dead front surface layer due to heavily doped emitter, high reflectance loss and ARC absorption.
Amorphous silicon (a-Si)	Absorption in the transparent conducting oxide (TCO) layer and recombination due to heavily doped semiconducting layers
Dye-sensitized cell (DSSC)	Limited by narrow active absorption range of the dyes used.
Cadmium Telluride (CdTe)	Absorption in buffer, typically in CdS and TCO layers.
Organic Cell	Loss associated with the electron-hole pair separation which results in recombination at the interface.

These loss mechanisms represent a practical limit to the maximum efficiency that can be achieved by the solar cell. The potential remains to increase cell efficiency by making better use of short wavelength radiation. One way to do that is to improve the electrical properties of the existing solar cells. For example in crystalline silicon PV cells, one can use an advanced design process, such as a lightly doped emitter [Shetty et al., 2013] to reduce the surface recombination and thus improving solar cell output or thin window layers [Cuony, 2011] which significantly decreased the reflection losses hence increasing the solar cell efficiency. Another example is the implementation of the third-generation PV structures such as multijunction or hetrojunction solar cells [Bedair et al., 1979, Ramanathan et al., 2005] in which cells with increasing band gap are stacked on top of each other. Each cell absorbs a different part of the solar spectrum and the sum of the output from these cells can boost the overall efficiency.

The focus of this chapter is a potential solution by plasmonic coupling of silver nanoparticles (Ag NPs) and luminescent materials to convert high energy photons into lower energy before the interaction with the solar cells occurs - a process referred to as plasmonic luminescent down-shifting (pLDS) [Ahmed, 2015, Ahmed et al., 2016a]. This is a new approach for a LDS layer utilizing plasmonic interaction in a composite layer of luminescent species incorporated with metal nanoparticles (MNP) such as Ag NPs. The addition of pLDS composite layers containing core–shell quantum dots CdSe/ZnS was demonstrated to increase

the short circuit current density (J_{sc}) of c-Si and DSSC devices between 300 and 500 nm, where the QDs is most absorbing. Up to ~22% (relative) increase has been achieved for both cells when compared with cells with no pLDS layers. The LDS process however is not a new approach, it has been discussed thoroughly in literature review. It involves a luminescent species that is applied in a transparent polymer/glass host material on top of the PV cell [Hovel et al., 1979, Strümpel et al., 2007, Klampaftis et al., 2009; 2012, McIntosh et al., 2009, Le Donne et al., 2009; 2011, Rothemund et al., 2011, Klampaftis and Richards, 2011, Ma et al., 2013, Ross et al., 2014, Alonso-Álvarez et al., 2014, Ahmed et al., 2016b]. Other techniques for LDS have recently been investigated where the luminescent species can be sprayed on top of the cells using a spray coating technique [Chander et al., 2015] or can be incorporated into a multifunctional coating system based on a photocurable fluoropolymer [Bella et al., 2015; Griffini et al., 2015]. Such a coating system has allowed for significant improvement of the power conversion efficiency of uncoated DSSC devices and has also improved the cell stability and prevented photochemical and physical degradation.

MNP exhibiting surface plasmon resonance (SPR) have been shown to enhance the optical properties of many types of lumophores [Ford & Weber, 1984, Reisfeld et al., 2010, Chandra, 2013]. In this chapter and for the first time pLDS layers containing core–shell quantum dots CdSe/ZnS were fabricated and applied on top of CdTe mini-modules produced at a larger scale of 15x15 cm. Prototypes developed for pLDS/CdTe devices have shown significant enhancement in generated photocurrent at short wavelengths 300-500 nm. At these wavelengths, the pLDS composite layer has shown to increase the J_{sc} by 63.6% using an AM1.5G ASTM standard solar simulator. In the following sections, the background theory into luminescent processes and plasmonic interaction will be presented and the luminescent materials investigated in this study will be discussed. Also the pLDS devices fabrication process and electrical characterisation will be presented.

1.1 Luminescence Phenomena

Luminescence is the emission of light from any substrate and occurs from electronically excited states [Lakowicz, 2006a]. Depending on the nature of the excited state, the luminescence can be either fluorescence or phosphorescence. In phosphorescence, the emission of light is from triplet excited states in which the electron in the excited orbital has the same spin orientation as the ground-state electron. In fluorescence, the electron is in the excited singlet state and it is paired in the excited orbital to a second electron in the ground-state orbital. The fluorescence emission rate is of the order of 10^8 s^{-1} with very short lifetime of the order of 10 ns, while phosphorescence lifetimes are typically of the order of a millisecond to a second and a low emission rate of 10^3-10^0 s^{-1}. The processes of fluorescence and phosphorescence are illustrated by the Jablonski diagram in figure 3, where the singlet ground, first and second electronic states are depicted by S_0, S_1 and S_2 respectively [Lakowicz, 2006a].

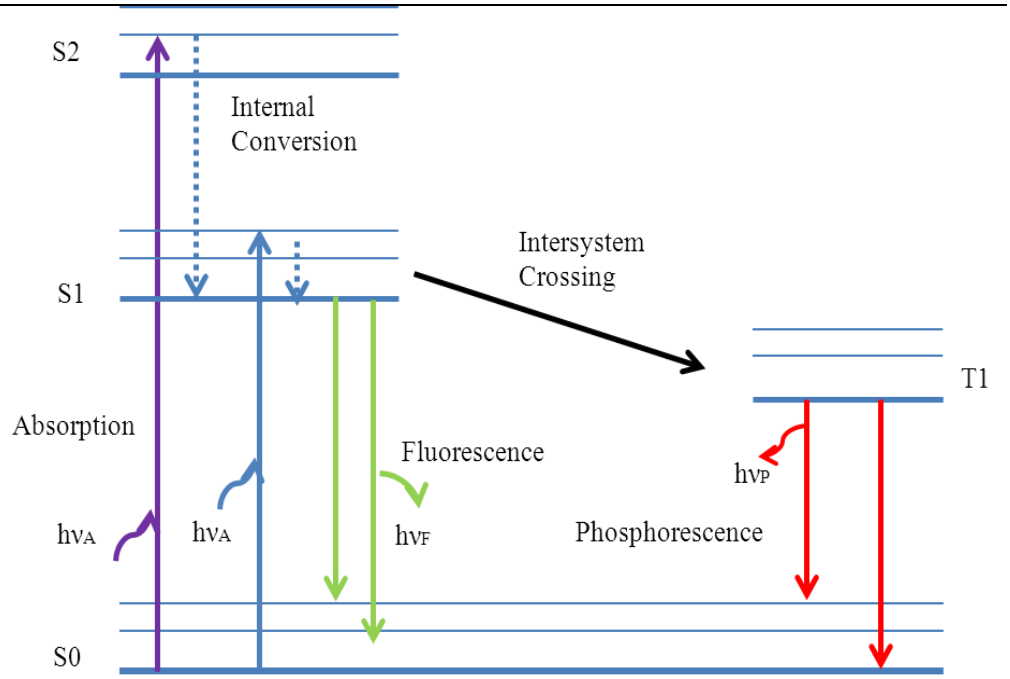

Figure 1: One form of Jablonski diagram, the singlet ground, first and second electronic states are depicted by S_0, S_1 and S_2 respectively.

When a photon is absorbed by a fluorophore, an electron can be excited to some higher level of either S_1 or S_2 after which it relaxes to the lowest vibrational level of S_1. This process occurs within 10^{12} s^{-1} (less than the fluorescence lifetimes) and is called internal conversion. Therefore, the fluorescence emission generally results from a thermally equilibrated excited state that is the lowest energy vibrational level of S_1. The molecules in the S_1 state can possibly undergo a spin conversion to the first triplet state (T_1 in Figure 1) after which the emission from the T_1 state is phosphorescence and the conversion process form S_1 to T_1 is called intersystem crossing. Molecules containing heavy atoms such as rear earth complexes are frequently phosphorescent. They facilitate intersystem crossing and thus enhance phosphorescence quantum yields [Lakowicz, 2006a].

1.2 Luminescent Down–Shifting Process

Luminescent Down-Shifting (LDS) is a purely optical approach to increase the ultra-violet/blue response of a solar cell by shifting short wavelength light to longer wavelengths for which the external quantum efficiency (EQE[1]) of solar cell is higher [Hovel et al., 1979, Strümpel et al., 2007, Klampaftis et al., 2009, McIntosh et al., 2009, Rothemund et al., 2011, Ross et al., 2014, Alonso-A´lvarez et al., 2014, Ahmed et al., 2016b]. In the device, luminescent materials convert high energy photons to lower energy, as illustrated in figure 4, before

[1] EQE is the ratio of the number of charge carriers that are collected by the solar cell to the number of photons of a given wavelength entered into the solar cell [Hu & White, 1983].

interaction with the solar cells occurs. High energy photons are re-radiated at a longer wavelength, better matching the photosensitivity spectral response of the CdTe solar cell.

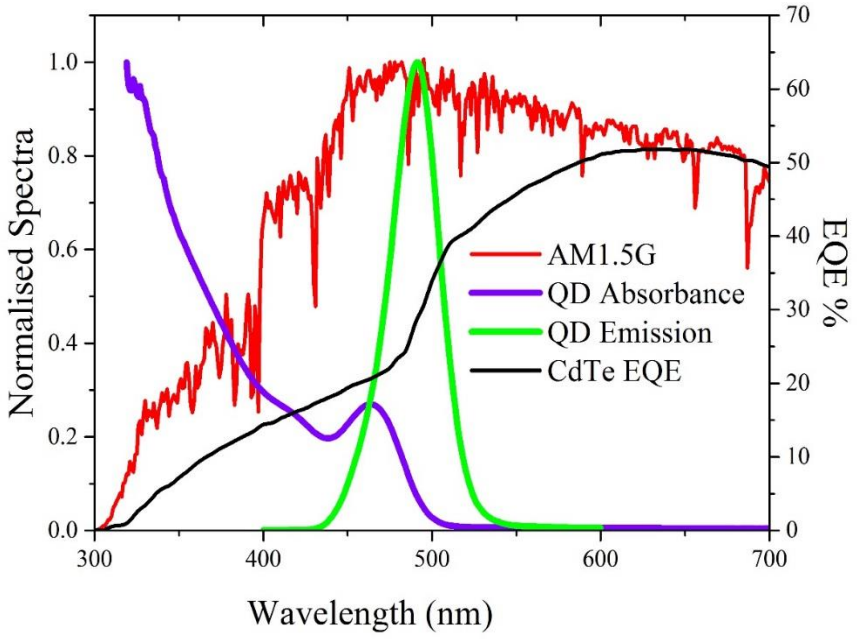

Figure 2: LDS processes to increase solar cell active range and efficiency. Normalized absorbance and emission spectra of QD-490, along with the AM1.5G solar spectrum and the EQE of CdTe PV module.

As can be seen in figure 4 CdTe solar cell exhibits a sharp decrease in response for wavelengths less than 550 nm. A fluorescent materials such as QDs , which absorbs light between 300 to 500 nm and emits at 500 nm shifts the incident light from where the cell has a poor optical response (at short wavelengths) to where the EQE of the cell is higher (at longer wavelengths). As a result of the luminescent process, more electron-hole pairs can be created in the solar cell for a given number of incident photons and a higher short-circuit current (Isc) is generated.

The first research using LDS layers "on top of'' PV cells was by Hovel et al., [1979]. However, the concept of LDS (i.e. the enhancement of the short wavelengths response of PV devices) appears frequently in the literature in the late 1970s, when LDS was utilized for an optical concentration process in so-called luminescent solar concentrators (LSC) [Weber & Lambe, 1976, Goetzberger & Greubel, 1977, Levitt & Weber, 1977]. The typical LSC consists of a flat plate containing a luminescent dye. The PV cell is placed on one of the plate edges. The other three edges and the back of the plate are mirrored to ensure that light can only emerge either at the top surface or where the PV cell is placed. This allows a certain wavelength to be absorbed by the luminescent dye and re-emitted isotropically. The emitted photons are wave guided to a reduced area of the photovoltaic cell at the plate edges.

In an LDS layer (in contrast to the LSC), there is no geometric concentration of the light, i.e. the area of PV cell is not reduced. The LDS layer is used to modify the incident spectrum only. The optical process involves an LDS layer positioned on top of a PV cell is illustrated in figure 5.

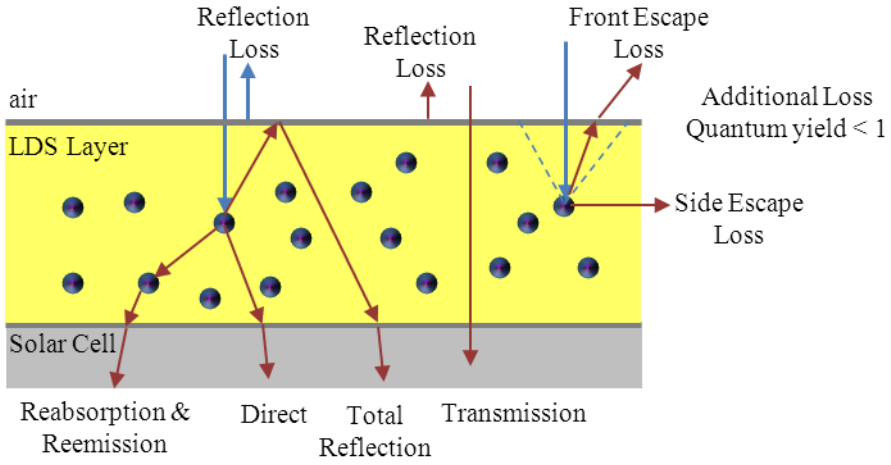

Figure 5: Optical process and optical losses in LDS layers on top of PV [Rothemund et al., 2011].

Incident solar radiation is absorbed and re-emitted at longer wavelength. The majority of the emitted radiation will be directly or following internal reflection at air/LDS interface or transmitted to the PV cell. Light could be re-absorbed and re-emitted by another luminescent species. Part of the luminescence will be lost from the PV cell through the top or the side of the LDS layer (the escape cone losses). Light could also be transmitted directly to the cell if is not absorbed by the luminescent species.

The introduction of an LDS layer in the PV cells creates additional interaction with the light which can result in extra loss mechanisms. These losses are caused either by the host materials or the luminescent species and can be summarised [Klampaftis et al., 2009] as;

I. Parasitic absorption from the host materials
II. Emission at less than unity luminescent quantum efficiency from the luminescent species.
III. Introducing an additional interface (i.e. the LDS layer) will increase reflection losses. If, however the solar cell has no or not good ARC, the addition of LDS layer in this case is beneficial and it can reduce the reflection losses.
IV. Photon emission losses through top and side planes of the LDS layer.
V. Luminescence quenching at higher concentration.
VI. Partial absorption by luminescence molecules of incident photons in the “visible” spectral region where cell EQE is relatively high.
VII. Scattering losses from the luminescent species at higher concentration.
VIII. Re-absorption of downshifted photons by luminescent molecules within the layer.

Therefore, any potential gain made by shifting the spectrum will have to compensate for these losses before showing an additional improvement. Important factors in deciding this are the following [Klampaftis et al., 2009 and Ross et al., 2012];

- Absorption of the luminescent materials where the EQE of the cell is poor and emission of the luminescent materials where the EQE of the cell is high
- Luminescent quantum yield of the material and its Stokes shift
- Front and edge escape cone losses, where light emitted by the luminescent material does not reach the cell
- Absorption in the new layers added to the solar cell in comparison to the exciting
- LDS refractive index should be comparable to the solar cell substrate to reduce internal reflection

1.3 Luminescent Materials for LDS Layers

An ideal luminescent species for LDS exhibits near unity luminescent quantum yield (LQY), a wide absorption band in the region where the PV cell external quantum efficiency is low, high absorption coefficient, a narrow emission band, good separation between the absorption and emission bands and low cost [Strümpel et al., 2007, Klampaftis et al., 2009]. The LDS layer host material must exhibit high transmittance and low scattering over the operating wavelength, and be a suitable environment for the dissolution of the luminescent species as well as have long term photostability [Rowan et al., 2008, Klampaftis et al., 2009]. A large number of luminescent materials have been investigated for their use as LDS layers [Strümpel et al., 2007, Klampaftis et al., 2009]. They can be separated into three main categories; organic dyes, rare - earth ion complexes and quantum dots.

Organic dye materials have been observed to have high absorption coefficient, close to unity LQY and easy dissolved in polymeric matrix [Swift & Smith, 2003, Earp et al., 2004a, Earp et al., 2004b, Slooff et al., 2005; 2006, Debije, 2007, Glaeser & Rau, 2007, Ahmed et al., 2012a, Ahmed et al., 2012b]. However, they commonly have narrow absorption bands [Debije, et al., 2008]. Rare earth ion complexes have a low absorption coefficient [Klampaftis et al., 2009]. Nevertheless, the use of an antenna structure which can absorb UV light and transfer the energy to the rare - earth ion for emission, improves their absorption and makes them suitable LDS materials [Bakker et al., 2000, Yanagida et al., 2000, Xiao & Selvin, 2001, Slooff et al., 2002, Hebbink, 2002, Werts et al., 2002a, Werts et al., 2002b, Faulkner et al., 2004, Shunmugam et al., 2005, Van Deun et al., 2006, Sardar et al., 2006, Leif et al., 2006, Marchionna et al., 2006, Li et al., 2008, Xu et al., 2008, Shavaleev et al., 2008, Debije et al., 2008; 2009, Goldschmidt et al., 2009, Ross et al., 2012; 2014, Binnemans, 2009, Le Donne et al., 2009; 2011, Van der Ende et al., 2009, Moudam et al., 2009, Wang et al., 2011a, Kennedy et al., 2015, Di Lorenzo et al., 2016]. The quantum dots which have been used for plasmonic coupling in this chapter is discussed below.

1.3.1 Quantum Dots

Quantum dots (QDs) have been extensively studied by several groups for their great promise and distinct spectroscopic properties [Mićić et al., 1997, Du et al., 2002, De Mello Donegá et al., 2003, Van Sark., 2006, Xu et al., 2007, Cheng et al., 2010, Wong et al., 2010,

Sadeghimakki & Sivoththaman, 2010, Xiaodong et al., 2011, Shirasaki et al., 2013, Ahmed et al., 2016a, Ahmed et al., 2016b]. QDs are nanoparticles of a semiconductor material, and are also known as nanocrystals. They are man-made structures composed of compound semiconductors like Cadmium Selenide, (CdSe), or Zinc Sulfide, (ZnS), and range from 2 to 10 nanometres in diameter (about the width of 50 atoms) [Gaponenko, 1998]. Because of their small size, quantum dots display distinct optical and electrical properties compared to the semiconductor in bulk form. Quantum dots are characterised by the emission of photons under excitation where the wavelength of these emitted photons depends not on the material from which the quantum dot is made, but its size, that is quantum confinement effect. The smaller the dot, the closer it is to the blue end of the spectrum (i.e. it will emit photons with higher energy at shorter wavelengths) and the larger the dot, the closer to the red end (i.e. it will emit photons with lower energy at longer wavelengths) [Gaponenko, 1998, Ethayaraja et al., 2007]. There are two main types of QDs:

- Core QDs which consist only of a core of semiconductor material such as Cadmium Telluride (CdTe) or Indium Phosphide (InP).
- Core-shell QDs which consist of a core with a shell of higher band gap materials as illustrated in figure 6. The capping layer provided in a core-shell structure is to avoid agglomeration of QDs and to increase their solubility in organic solvents.

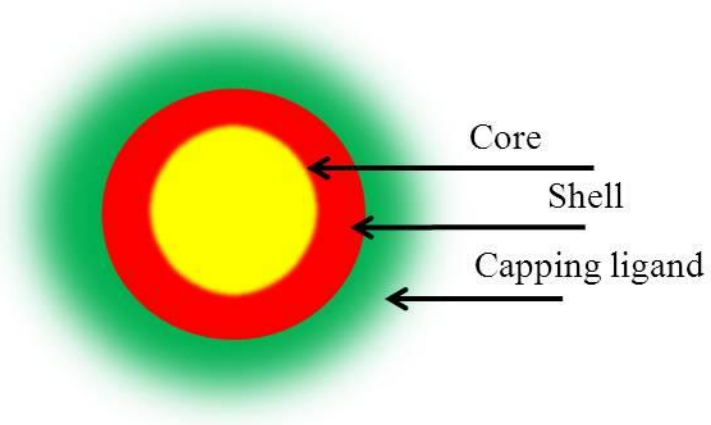

Figure 6: A Core-shell QDs structure with capping ligand.

The high surface-to-volume ratio of QDs, leads to the possibility of the photoexcited electron and hole getting trapped due to defects or impurities in the QDs core surface. These traps can lead to non-radiative recombination of the electron hole pairs and therefore degrade the optical and electrical properties of the QD. One approach to reduce these surface defects is to passivate the QD core with a shell of higher band gap material. The passivation of the core QDs reduces the effects of defects on the core surface, which leads to less non-radiative recombination and hence higher radiative recombination (i.e. luminescence) [Gaponenko, 1998, De Mello Donegá et al., 2003, Pickett & O'Brien, 2001, Jang et al., 2004].

QDs exhibit broad absorption spectra, high absorption coefficients and emission wavelengths which can be tuned according to their size as a result of quantum confinement [Van Sark et al., 2004, Ethayaraja et al., 2007]. They have been proposed for use in LSC instead of organic dyes [Chatten et al., 2003, Schüler et al., 2007, Sholin et al., 2007, Gallagher et al., 2007, Reda, 2008, Kennedy et al., 2009]. The advantages of QDs with respect to organic dyes are their high brightness and stability [Bruchez Jr et al., 1998]. However, they also suffer from re-absorption losses due to the overlap of their absorption and the emission bands [Klampaftis et al., 2009] which has resulted in low optical efficiency LSC devices. Majority of the currently available QDs are made of toxic materials (such as Cadmium), they are generally more expensive than fluorescent dyes at small scale production levels, and the commercial quantum dots are limited to 30-50% quantum yield [PlasmaChem GmbH, NanoCo Group]. However, high quality QDs with high photoluminescence quantum yields > 80% [De Mello Donegá et al., 2003] and up to 97% [Chen et al., 2013] have been achieved for quantum dots in a laboratory environment.

1.3.2 Host Materials

The most frequently used host material is the polymer poly(methyl methacrylate), also known as PMMA. Its main advantages are low cost and high optical clarity. Moreover, it is easy to process when doping with fluorophores [Maruyama et al., 2000, Rowan et al., 2008, McIntosh et al., 2009, Wilson, 2010]. Epoxy resin, poly-vinyl acetate (PVA) and poly-ethylene vinyl acetate (EVA) (which has been proven material in Si solar cell panel) are also commonly used as host materials [Marchionna et al., 2006, Li et al., 2008, Klampaftis et al., 2009, Daram et al., 2011].

As mentioned in section 1.2, the introduction of the LDS layer on top of a solar cell causes the additional loss mechanism of parasitic absorption from the host materials. This, however, strongly depends on the materials used and the thickness of the LDS layer. Epoxy resin has been shown to exhibit lower absorption in the visible region [Gallagher et al., 2007] and may therefore have lower parasitic absorption losses. It may also be advantageous as a host for luminescent species which may be sensitive to temperature rises caused by absorption of visible light. Most of the polymeric materials are highly transparent in the visible region but one of their main issues is the photo-degradation under UV exposure [Aboueiezz & Waters, 1978, Tanaka et al., 2006, Earp et al., 2010]. Inorganic materials such as Al_2O_3 or CaF_2 have been used as host materials [Hovel et al., 1979, Kawano et al., 1997] and also various types of glass and organic paint thinners [Maruyama et al., 2000, Maruyama & Kitamura, 2001, Švrček et al., 2004].

1.4 Solar Cell Spectral Response

The spectral response (SR) of a solar cell gives a ratio of the photocurrent generated by the solar cell to the power incident on the solar cell at each wavelength [Goetzberger et al., 1998]. A solar cell responds to a certain range of wavelengths. The response at longer wavelengths depends on the bandgap energy of the solar cell material, and at short wavelengths depends on absorption of the material [Goetzberger et al., 1998, Bentham Ltd, 2014]. Spectral response curves of selected solar cells are shown in figure 7, along with the AM1.5G solar spectrum.

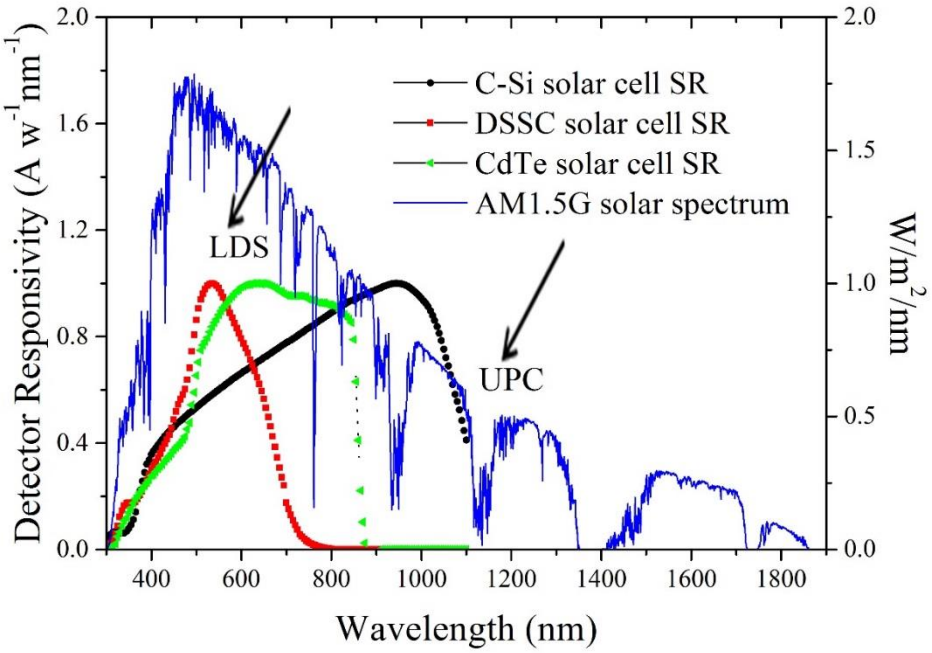

Figure 7: Spectral responsivity of c-Si, CdTe and DSSC solar cells along with AM1.5G solar spectrum.

It can be seen that, at short wavelengths below 400 nm, the cell response is very low whereas at intermediate wavelengths the cell response approaches the ideal. The response drops back to zero at longer wavelengths because the bandgap energy of the solar cell material is higher than the energy of the photons in this region of the solar spectrum. To overcome this limitation for longer wavelengths, luminescent up conversion (LUC) materials have been investigated [EPHOCELL project, 2013], which results in the combination of the energy of two or more photons of low energies to one photon with high energy [Wohnhaas et al., 2013].

In an ideal situation, the absorption spectrum of the solar cell materials should perfectly match the entire solar spectrum in order to convert the maximum photons from solar radiation to an electrical response. However, there is a large mismatch between the solar emission spectrum and the absorption properties of the currently used solar cell materials. At short wavelengths, each photon has a large energy, and therefore the ratio of photons to power is reduced. Any energy in excess of the band gap energy of the solar cell materials is not utilized by the solar cell and instead goes to heating the solar cell and is therefore wasted [Ferry et al., 2010, Bentham Ltd, 2014]. The LDS layers aim to convert non-absorbable solar radiation in the UV (290-400 nm) into absorbable incoming radiation in the visible (400-700 nm) via florescence phenomena, hence making better use of short wavelength radiation.

1.4 Plasmonic Interaction

As discussed in section 1.3, the addition of an LDS layer to the photovoltaic cell introduces additional loss mechanisms and therefore any potential gain made by shifting the spectrum will have to compensate for these losses before an improvement in performance can be achieved. The loss mechanisms have been discussed in section 1.3, (V) luminescence quenching at higher concentration, (VI) partial absorption by luminescence molecules of incident photons in the "visible" spectral region where cell EQE is relatively high, (VII) re-absorption of downshifted photons by luminescent molecules within the layer and (VIII) scattering losses from the luminescent species at higher concentration can be minimized by plasmonic interaction between metal nanoparticles (MNP) and luminescent species. Plasmonic materials have been incorporated in semiconductor devices including light emitting diodes [Pillai et al., 2006, Catchpole & Pillai, 2006] and silicon photodiodes [Lim et al., 2007]. Several research groups have studied applications of surface plasmonics in photovoltaic cells [Stenzel et al., 1995, Westphalen et al., 2000, Yakimov et al., 2002, Rand et al., 2004, Pillai et al., 2007, Morfa et al., 2008, Hägglund et al., 2008a, Hägglund et al., 2008b, Lee et al., 2009, Duche et al., 2009, Ferry et al., 2010, Yu et al., 2013, Chen et al., 2014, Xu et al., 2013] and in vacuum deposited thin film photovoltaic cells to enhance performance. In recent studies of plasmonic photovoltaic cells coupled with LSC, a large enhancement in device efficiency has been shown [Chandra et al., 2010, Reisfeld, 2010, Wang et al., 2011b, Wang et al., 2012, Chandra et al., 2012, Chandra et al 2013].

MNP exhibiting surface plasmon resonance (SPR) have been shown to increase the excitation and emission rate of luminescent species and, hence, photon absorption [Ford & Weber, 1984, Stranik et al., 2005, Tam et al., 2007, Fort & Gŕesillon, 2008, Reisfeld et al., 2009, Chandra et al., 2010; 2012, Chandra, 2013, Ren et al., 2015, Ahmed et al., 2016a]. Several groups showed an enhancement in the fluorescence intensity of QDs and organic dyes in the presence of silver and gold nanoparticles [Wilson, 1987, Reisfeld et al., 1988; 2010, Lakowicz et al., 2002, Farahani et al., 2005, Lakowicz, 2006b, Chandra et al., 2010; 2012, Chandra, 2013]. Also, some early research has shown an enhancement in the emission properties of rare-earth materials in the presence of metal nanoparticles [Reisfeld, 1983, Strohhöfer & Polman, 2002, Reisfeld et al., 2009. Li et al., 2016]. The presence of MNP has been shown to increase the fluorescence resonance energy transfer [Wokaun et al., 1983, Lakowicz et al., 2002], and fluorescence emission directionality [Andrew & Barnes, 2000; 2004]. It has also been shown to increase the luminescent quantum yield and photostability of many types of lumophores [Novotny, 1996, Enderlein, 2001, Strohhöfer & Polman, 2002, Lakowicz et al., 2002, Farahani et al., 2005, Musken et al., 2007]. The introduction of MNPs has therefore opened up the use of many types of lumophores such as quantum dots, rare-earth complexes and organic dyes which have previously been rejected for inclusion in LDS layers because of their low quantum yield, low absorption coefficient and poor photostability [Ahmed, 2015].

The optical response of metal nanoparticles and their interaction with luminescent species can be investigated by optical measurement of absorption and emission. The main challenge, however, is controlling the composite structure to achieve maximum enhancement. Plasmonic interaction can be controlled [Chandra, 2013] by orientation of the luminescent species with respect to the MNP surface, the surface plasmon resonance wavelength of MNPs, the spacing between MNP and luminescent species and/or the spectral overlap of the SPR with the absorption and emission bands of the luminescent species.

1.4.1 Surface Plasmon Resonance and Extinction

Surface plasmons are charge density waves that propagate along the surface of some metals such as gold and silver and result in a strongly enhanced local oscillating electromagnetic field (EM). When a particle of size *d* is under the action of such an EM, (considering that *d* is less than the wavelength of the EM) the wavelength can set up standing resonance conditions, as represented in figure 8 and the electrons in the conduction band start to oscillate, transforming energy from the incident EM waves into different forms of energy such as thermal in an absorption process or radiate energy in a scattering process [Bohren & Huffman, 1983, Prasad, 2004, Maier, 2007]. The attenuation of an EM wave by absorption and scattering as it is going through a material is known as extinction [Bohren & Huffman, 1983]. The optical or surface plasmon resonance frequency condition is determined by measuring the extinction and was found to be dependent on the shape, size, and dielectric constants of the metal [Link & El-Sayed, 2000, Kelly et al., 2003, Calander & Willander, 2002, Eustis & El-Sayed 2006, Fort & Gŕesillon, 2008].

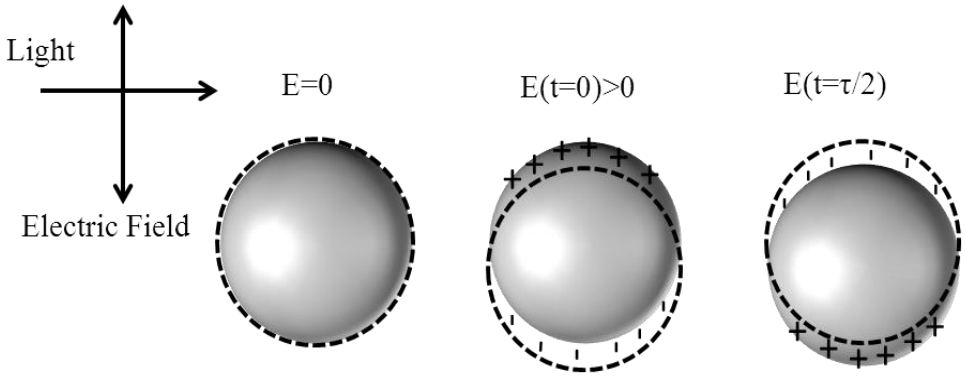

Figure 8: Schematic diagram of surface plasmon resonance due to interaction of the electrons in the conduction band of a metal sphere in the absence (left) and presence (center and right) of external electromagnetic field [Ahmed et al., 2016a].

The electric field of the incoming light wave (figure 8 centre and right) induces a polarization of the free electrons in the conduction band with respect to the much heavier ionic core of the spherical nanoparticle. In the presence of this electric field, the positive charges are assumed to be steady and the negative charges are moving. The collective oscillation of these electrons is known as the dipole plasmon resonance of the particle. Therefore, when the nanoparticle is placed in an electric field, the negative charges are displaced with respect to the positive ones. The displacement and the separation between charges results in a net charge difference at the nanoparticle boundaries which gives rise to a restoring force against the positive ions and hence surface plasmon oscillation is created. SPR is therefore known as a coherent electronic excitation of all the "free" electrons at the surface of the metal which gives rise to surface plasmon resonances [Bohren & Huffman, 1983, Prasad, 2004, Maier, 2007]. The SPR is different for nanoparticles with an anisotropic surface distribution such as nanorods,

triangular and spheroid. In such materials, the SPR consists of a transverse SPR and longitudinal SPR, corresponding to the distribution of electrons perpendicular and along the symmetry axis [El-Sayed, 2001, Hutter & Fendler, 2004, Eustis & El-Sayed, 2006]. The SPR for nanoparticles anisotropically distributed is created from multipolar plasmon oscillation of electrons and the only difference between that and the dipolar plasmon is the shape of the surface charge distribution on the nanoparticle surface [Ghosh & Pal, 2007]. Such as in the quadrapole mode half of the electron cloud moves parallel to the applied field and the other half moves anti-parallel. This indicates the importance of the surface in SPR, because it alters the boundary condition for the polarizability of the metal [Ghosh & Pal, 2007]. A number of metals such as Ag, Au, Al and Cu, [Bohren & Huffman, 1983, Chan et al., 2007; 2008] support SPR which can be tuned in nanoparticles throughout the UV/Visible- near-IR spectrum. Ag and Au nanoparticles are the most established and studied because they are stable and their SPR is in the visible range. In Ag the plasmon frequency is also influenced by the d-orbital electrons, thus making it difficult to calculate the plasmon frequency from electronic structure calculations.

The optical properties of the MNP are described by their dielectric function, ε. The Quasi-Static approximation of Mie's theory [Mie, 1908] for scattering and absorption of light of wavelength λ, by spherical particles is employed to relate the dipole plasmon frequency of MNP to the dielectric function and to understand the optical response of MNP to an electric field. It assumes that the nanoparticles are much smaller than the wavelength of the incident light and the electric field on the particles is uniform. Under these circumstances, the interaction is governed by electrostatics rather than electrodynamics; the scattering cross section is given [Bohren & Huffman, 1983] by;

$$\boldsymbol{\sigma_{scat} = \frac{1}{6\pi}\left(\frac{2\pi}{\lambda}\right)^4 |\alpha|^2} \qquad \text{Equation 1}$$

where α is the polarizability of the particles, which describes how the sphere is polarised by the applied field [Bohren & Huffman, 1983], and it is given by;

$$\boldsymbol{\alpha = 4\pi a^3 \frac{\varepsilon_i - \varepsilon_s}{\varepsilon_i + 2\varepsilon_s}} \qquad \text{Equation 2}$$

Here, a is the radius of the nanoparticles, ε_i and ε_s are the dielectric constants of the particles and surrounding medium, respectively. The dipole moment p that is induced in the sphere by the external electric field E_0 is given by;

$$\boldsymbol{\hat{p} = \alpha\varepsilon_s \widehat{E_0} = 4\pi\varepsilon_s a^3 . \frac{\varepsilon_i - \varepsilon_s}{\varepsilon_i - 2\varepsilon_s} \widehat{E_0}} \qquad \text{Equation 3}$$

The resonance wavelength occurs when $\varepsilon_i = -2\varepsilon_s$, this happens when the polarizability is at a maximum and the particles then exhibit the so-called dipolar surface plasmon resonance or short surface plasmons [Ghosh & Pal, 2007, Fort & Gŕesillon 2008]. The absorption cross-section of the sphere scales with the polarizability as well and is given [Bohren & Huffman, 1983] by:

$$\boldsymbol{\sigma_{abs} = \frac{2\pi}{\lambda} \lim[\alpha]}$$ Equation 4

The resonance dipolar behaviour is not limited to spherical particles; a wide range of metal nanoshapes exhibit similar behaviour. When the size of the nanoparticles increases a series of SPR peaks can appear in the optical spectrum this is due to the excitation of the higher plasmonic wave modes such as the electric quadrupole modes or the magnetic dipole modes in the metal nanoparticle. In plasmonic solar cell applications, the light absorbed in the metal is not useful in the photocurrent generation and therefore it is important in the design to keep $\sigma_{scat} >> \sigma_{abs}$ in order to reduce the metallic losses [Ferry et al., 2010].

1.4.2 Plasmonic Interaction between MNP and Luminescent Species

As discussed previously, the fluorescence process consists of absorption of a photon and subsequently emission of a photon at longer wavelengths. The optical properties of fluorescent species were reported to exhibit dramatic spectral changes in the presence of metal nanoparticles [Noguez, 2006, Ghosh & Pal, 2007, Fort & Gŕesillon 2008, Catchpole & Polman, 2008]. SPR of metal nanoparticles amplifies the incident electric field intensity around NPs, acting as an antenna to a receiver and creating an enhanced electromagnetic field [Stranik, 2007, Chandra, 2013]. The enhanced electric field vector decays exponentially away from the surface [Lakowicz et al., 2002, Stranik, 2007, Chandra, 2013], and therefore it is important to place the fluorescent species at a distance where the enhanced electric field is present.

Theoretically, a fluorescent material can be represented as oscillating electric dipole, (p_{exc}). When the incident light is not excessively strong and fluorophore molecules are not in saturation, the absorption rate is proportional to the intensity of light and to the molecule absorptivity (ϵ) of the fluorophore molecule [Fort & Gŕesillon, 2008]. The absorption rate of the fluorophore molecule depends on its orientation with respect to the exciting electric field. The fluorophore molecules will not be excited if their dipole moment is perpendicular to the electric field vector. The average excitation rate of the fluorophore molecule can therefore be given as [Fort & Gŕesillon, 2008];

$$\boldsymbol{\Gamma_{exc} \propto \epsilon(\lambda) |\, \hat{p}_{exc} . E_0|^2}$$ Equation 5

In the case of placing a nanoparticle close to a fluorescent material, an electrical field E_1 will be generated by the nanoparticle replacing the incident electric field E_0 in equation 5. The excitation enhancement factor,R_{exc} , which is due to the enhanced local electrical field around the nanoparticle, is defined as [Fort & Gŕesillon, 2008];

$$\boldsymbol{R_{exc} = \frac{|\, \hat{p}_{exc} . E_1|^2}{|\, \hat{p}_{exc} . E_0|^2}}$$ Equation 6

The excitation enhancement factor depends on the dipole orientation and particle size. For smaller particles, around 10 nm, the enhancement was reported to be very large and, as the size of the particles increases, the enhancement decreases [Stranik, 2007]. The excitation enhancement also depends on the distance between the nanoparticles and the fluorophore. The

enhancement decreases with increasing distance of the fluorophore from the nanoparticle [Lakowicz et al., 2002, Fort & Gŕesillon, 2008]. The excitation enhancement reaches maximum if the SPR energy overlaps with that of the absorption of the fluorophore [Stranik, 2007].

The emission properties of a fluorophore such as quantum yield can also be changed due to plasmonic interaction. Quantum yield for a fluorophore in the presence of MNP is given by [Fort & Gŕesillon, 2008];

$$\boldsymbol{Q_m = \frac{\Gamma_r+\Gamma_m}{\Gamma_r+\Gamma_m+\Gamma_{nr}+\Gamma_{mnr}}} \qquad \text{Equation 7}$$

where Γ_r and Γ_{nr} are radiative and non-radiative decay rates while Γ_m and Γ_{mnr} are the new radiative and non-radiative decay rates in the presence of the nanoparticle [Anger et al., 2006, Fort & Gŕesillon 2008]. The value of Q_m varies from 0-1 for non-fluorescing materials to highly fluorescent, respectively. Equation 1.8 suggests that high quantum yields can be obtained whenever Γ_m is comparable to Γ_{nr}. As Γ_m becomes larger than Γ_r , the emission of the fluorophores and hence the quantum yield is increased. The increase of Γ_m is more effective for fluorescent materials with low quantum yield, meaning the enhancement is not significant for materials with high quantum yield [Fort & Gŕesillon, 2008].

The sum of the radiative decay rate and the non-radiative decay rate gives the total decay rate $\Gamma = \Gamma_r + \Gamma_{nr}$. The fluorescence rate can be written as [Fort & Gŕesillon, 2008];

$$\boldsymbol{\Gamma_{fluo} = \Gamma_{exc}\,\frac{\Gamma_r}{\Gamma}} \qquad \text{Equation 8}$$

where Γ_{exc} is the excitation rate from equation 6 which depends on the local excitation field, E_0. From equation 8, it follows that the fluorescence rate is a function of both excitation

and emission. Emission enhancement for a fluorescent material is accomplished if the modified quantum efficiency is larger than the initial quantum efficiency of the material and reaches its maximum if the SPR energy overlaps with that of the fluorophore emission [Stranik, 2007].

The fluorescent molecule can also be described as an oscillating dipole at the emission wavelength. When the molecule is placed into the enhanced electric field of the MNP; the energy from the molecule is coupled to the surface of the MNP and then re-radiates the energy into the vicinity. The emission enhancement is expressed by [Stranik, 2007];

$$\boldsymbol{R_{em} = \frac{Q_m}{Q}} \qquad \text{Equation 9}$$

The emission enhancement strongly depends on the quantum efficiency and on the distance between the MNP and the fluorescent material. The non-radiative decay rate in the approximation of small distance of nanoparticle and fluorescent material is given by [Kümmerlen et al., 1993];

$$\boldsymbol{\Gamma_{mnr} = \frac{\Gamma_r\, A}{l^3}} \qquad \text{Equation 10}$$

where, *A* is constant and *l* is the nanoparticle- fluorescent material separation. If l is very small (a few nanometre), the non-radiative decay rate becomes very large and the quantum yield value in equation 9 will drop to zero. The presence of MNP increases the radiative decay rate which enhances the emission rate of the fluorescent material leading to an increase in quantum yield. This enhancement is strongly dependent on the distance between the MNP and the fluorescent material. Equation 10 therefore, can be re-written as follows;

$$\Gamma_{fluo} = \Gamma_{exc} \frac{l^3}{A} \frac{\Gamma_{mnr}}{\Gamma} \qquad \text{Equation 11}$$

The typical distance has been optimised by Stranik, 2007 and was found to be around 10 nm.

1.4.3 Surface Plasmon Resonance in Silver Nanoparticles

Silver Nanoparticles plasmonic response depends on the size, shape, dielectric environment and on mutual electromagnetic interactions among particles in close proximity as was discussed in the previous section. SPR of Ag NPs with high symmetry like spheres and ellipsoids can be easily calculated with good fitting to experimental UV-vis spectra using the Mie theory and it can also be used to evaluate the average size of the particles [Amendola, et al., 2009]. The most commonly used numerical method to calculate the SPR of metal nanoparticles of lower symmetry is the discrete dipole approximation (DDA). This method has been used to calculate the extinction cross section of metal nanoparticles of arbitrary shape and nanometre size [Noguez et al., 2007]. Ag NPs have more intense and sharp plasmonic resonance than Au and Cu nanoparticles due to the small overlap of the SPR and the interband transitions of Ag [Kreibig, 1995].

Ag NPs that have been synthesized for this work are of spherical and triangular prism structures. The spherical particles fabricated were less than 40 nm in size therefore we have not observed any quadrupole resonance. The plasmon resonance wavelength is red shifted if the particle size is increased above 40 nm this is due to the additional electromagnetic effects in the nanoparticle [Kelly et al., 2003]. The extinction efficiency i.e. the ratio of the extinction cross section to the area of the sphere can be obtained from the Quasistatic theory. DDA calculations for both perfect and snipped prisms have been done by Kelly et al., (2003). Figure 9a shows the optical spectra of a 10 nm snipped triangle, each spectra representing the polarization along each principal axis of the prism. The in-plane polarization leads to peaks at 460 and 670 nm and the out of plane polarization leads to peaks at 335 and 430 nm. For an unsnipped prism the result is analogous to the snipped prism, the polarization vectors for the 770 nm is analogous to the dipole resonance with the largest induced polarization occurring at the tips of the prism. For the 460 nm the dipoles at the tip are opposite to the incident polarization direction, this pattern resembles that of a quadrupole as can be seen in Figure 10. The resonances at 770 and 460 nm are dipole and quadrupole plasmon resonances associated with in-plane polarization. The triangular prisms we have synthesized were about 50 nm. A decrease in the size of the prism leads to a red shift of the SPR peak [Wu et al., 2015] but we

observed the three distinct SPR bands corresponding to the in-plane dipole, quadrupole and out of plane quadrupole plasmon resonances as can be seen in Figure 9b.

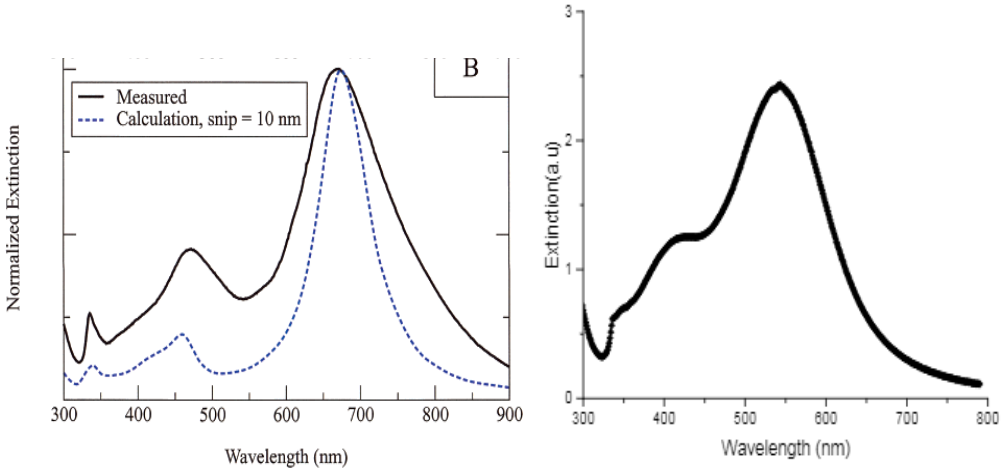

Figure 9: (a) UV-vis spectra of triangular Ag prisms with side length 100nm, snip 10 nm, along the three primary symmetry axes [Kelly et al., 2003] (b) UV-vis spectra of 50nm edge perfect triangular prisms as measured showing three SPR bands.

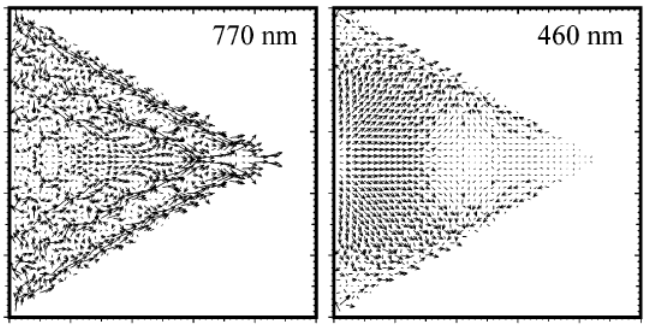

Figure 10: polarization vectors for dipole and quadrupole plasmon resonances at 770 and 460 nm respectively [Kelly et al., 2003].

1.4.4 Silver Nanoparticles – State of the Art

Silver nanoparticles in particular have been the interest of much scientific research since the discovery of their amplifying effects in Raman spectroscopy, giving rise to the field of Surface Enhanced Raman Spectroscopy (SERS) [Creighton et al., 1979, McNay et al., 2011]. Since then, studies have been carried out for different ranges of applications [Henglein, 1989, Lakowicz et al., 2004, Aslan et al., 2004; 2005, Wu et al., 2005, Catchpole & Pillai, 2006, Daghestani & Day, 2010, Iranifam, 2016, Cho et al., 2015] indicating unique optical properties associated with surface plasmon resonance.

The field of plasmon enhanced photovoltaics in particular is of much recent interest because of the light localization properties of metal nanoparticles [Peumans et al., 2003, Catchpole & Polman, 2008, Escoubas et al., 2011]. The first studies to explore the use of silver nanoparticles in solar cells were reported by Stuart & Hall in late 1990 [Stuart & Hall, 1998]. The authors showed an enhancement in the photocurrent of a factor of 18 for a 165 nm thick Si layer on a layer of SiO_2 photodetector at a wavelength of 800 nm when silver nanoparticles were used on the surface of the device. Westphalen et al., [2000] showed an enhancement of the short circuit photocurrent for silver clusters incorporated between an ITO and ZnPc structure organic solar cell. Yakimov & Forrest [2002] reported a 2.5% increase in the power efficiency for a tandem PV cell of multiple layers separated by silver nanoparticles, compared to 1.1 % for a single junction cell of same material. Experimental and theoretical studies by Catchpole & Pillai, [2006] have shown an enhancement of a factor of 8 in the electroluminescence from a silicon-on-insulator light-emitting diode at 900 nm using silver nanoparticles. A study by Pillai et al., [2007] showed overall increases of 33% in the photocurrent for silver nanoparticles deposited on a 1.25 mm thick silicon-on-insulator solar cell and 19% for planer wafer based cells. Catchpole & Polman, [2008] shown theoretically for a Si substrate, Ag particles can lead to path length enhancements up to a factor of 30 for optimised shapes. In their investigation, they have shown that the particle shape is a crucial parameter in designing plasmon enhanced solar cells and determines the light trapping efficiency [Catchpole & Polman, 2008, Ferry et al., 2010].

The incorporation of silver nanoparticles in GaAs photovoltaic cells has led to an increase in the optical path of the incident light in the absorber layers resulting in an 8% increase of current density of the cell [Nakayama et al., 2008]. Morfa et al., [2008], reported an efficiency increase of a factor of 1.7 for organic bulk hetrojunction solar cells. Temple et al., [2009] deposited a 10 nm silver nanoparticle layers on a Si solar cell surface followed by thermal annealing. A relative increase of 6.5% in the efficiency of the cell was calculated, but this increase is believed to be due to an improvement in the long-wavelength spectral response, which is related to the annealing and not to the presence of silver nanoparticles in their devices. In contrast, Pala et al., [2009] shown theoretically an enhancement of 43% in the absorption of a 50 nm Si substrate as a result of incorporation of a grating of silver nanoparticles on top of the surface.

Enhanced absorption of light up to 50% in a 50 nm blend layer, including spin-coated silver nanoparticles in organic solar cells was experimentally obtained by Duche et al., [2009].

Chuanhao et al., [2012], greatly enhanced the absorption in a sandwich structure of a-Si: H by 48% under AM1.5 illumination. This was achieved by designing a lower light-trapping structure with an Ag pyramidal array and an upper impedance-matching structure with an ITO pyramidal array. Dunbar et al., [2012], calculated the absorption in a 60 nm thick organic semiconductor film and it was found to be enhanced by up to 19% when silver nanoparticles with 60 nm widths uniformly dispersed on the film with a periodicity of 330 nm. A similar effect was shown by Shan et al., [2014], who investigated the effect of silver nanotubes on the absorption of organic solar cells using the finite element theory method and their calculations demonstrated an enhancement by up to 55% with respect to the bare cell.

Yu et al., [2013], drop cast silver nanoparticles which were dispersed in ethyl alcohol on the surface of poly-crystalline silicon (pc-Si) solar cell. The energy conversion efficiency increased by 2.8% and the short circuit current increased by 1.4%, compared to a pc-Si solar

cell without silver nanoparticles layers. The enhancement was found to depend on the Ag NP concentrations on the surface.

Cui et al., [2014], applied an intermediate layer of Ag in copper zinc tin sulfur (CZTS) solar cell between the absorber layer of the cell and the back contact interface. The Ag layer improved the absorbance of the absorber and significantly increased the solar cell electrical characteristics. Moreover, it reduced the series resistance from 19.5 to 12.8 $\Omega.cm^2$. A relative increase of 91% in the efficiency was achieved for the CZTS solar cell.

Research based on Ag nanowires in Polymer solar cells (PSCs) have been reported by Yang et al., [2014]. Ag nanowires were incorporated at the interface of the anode buffer layer and the active layer in the solar cell. This resulted in an increase of the short-circuit current density and the power conversion efficiency by 24% and 18% respectively under AM1.5 illumination.

Theoretical work has been reported by Karatay et al., [2014], in which they reported that placing silver nanoparticles on top of an organic solar cell could yield an enhancement in short circuit current density of 31% when an 80 nm thick active layer is used, resulting in an absolute increase in power conversion efficiency of 2% with respect to a device with no silver nanoparticles.

The use of silver nanoparticles to improve the fluorescent intensity of dyes has also been reported for LSC [Wilson, 1987]. A recent study on LSC was reported by Reisfeld, [2010], in which the effect of silver nanoparticles on the collection efficiency of LSC plate was a 12% increase compared to a plate without silver nanoparticles. Wang et al., [2011b], coupled an LSC plate of Lumogen Red dye with an organic solar cell with plasmonic silver nanoparticles and a factor of 2 enhancement of conversion efficiency was obtained when the absorption peak of the solar cell was tuned to match the emission peak of the Red dye.

Silver nanoparticles were also used to enhance the emission of luminescent materials. Many have reported an increase in the emission for different luminescent dyes in sol-gel films in the presence of silver nanoparticles [Reisfeld et al., 1988, Lakowicz, 2006b, Reisfeld et al., 2009]. By varying the size and shape of the Ag NPs the optical properties can be manipulated. [Hsu et al., 2015] embedded various types of Ag NPs in organic and perovskite photovoltaic cells. They found an increase in the short circuit photocurrent density by 7.6-17.5% and the power conversion efficiency by up to 13%.

Liu et al., [2014] have obtained an enhancement of 21.7% for a polymer solar cell (PSC) with a power conversion efficiency of 9.2% compared to a reference PSC cell. In their devices Ag NPs of different sizes were put in the anode buffer layer and the active layer to trigger the localized surface plasmonic effect and that resulted in the enhancement of the EQE of the PSC solar cells.

Ho et al., [2016] fabricated plasmonic Si solar cells with a matrix of Ag NPs surrounded by indium nanoparticles (In NPs) and they examined the plasmonic modulated light scattering induced by the Ag NPs/In NPs matrices. A 9.93% increase in short circuit current density and a 10.12% increase in conversion efficiency was measured for the fabricated plasmonic Si- solar cells.

Also, Al-Azawi et al., [2016] have mixed an organic dye with and without the mixture of silver and gold alloy NPs and these was incorporated in a TiO_2 film to use as photoanode in dye sensitized solar cells. The results confirmed the plasmonic enhancement effects the DSSC solar cells with the Ag-Au alloy NPs. It has yielded a power conversion efficiency of 5.81%, which was ~8.4% and 52.1% higher than that of the DSSC with Au NPs and the reference cell, respectively.

Most of the work reviewed above involved the implantation of the nanoparticles within the devices or solar cells inside the charge-selecting interfacial layers or blended with the solar cell active layer. This chapter howevr uses pLDS layers, in which the fabrication of Ag NPs and QDs composite layers was achieved and layers were deposited on top of a larger scale devices CdTe (15x15 cm). The enhancement in photocurrent and external quantum efficiency for the fabricated devices is reported in the following section.

1.5 pLDS Layers Fabrication

This section is focused on the characterisation of plasmonic luminescent down shifting layers for their inclusion on mini-modules CdTe devices. The plasmonic interaction between luminescent material QDs and Ag NPs incorporated into PMMA composite layers is investigated. The optimum concentration of Ag NPs which gives the maximum fluorescent enhancement is examined.

Plasmonic enhancement of fluorescence species have been shown to strongly depend on the spacing between MNP and fluorescence species [Chandra et al., 2012, Chandra, 2013]. There are two enhancements due to the presence of silver nanoparticles (i) an increase of the excitation rate and (ii) an increase in LQY [Stranik, 2007]. Both are a function of the plasmonic resonance of Ag NP. The enhancement is maximised for excitation if the SPR resonance overlaps with the excitation peak wavelength of the luminescent material while the enhancement is maximised for LQY if the SPR resonance overlaps with the peak emission wavelength. At the SPR resonance, MNP produced a strong enhanced electrical field around the MNP surface [Fort & Gŕesillon 2008]. In order to modify the luminescent material absorption and excitation rate it is important to place the luminescent material in the range of this electrical field to experience the plasmonic interaction.

The luminescent particle has to be placed at a distance where the maximum enhancement could be achieved. If the luminescent material is placed at a smaller distance, the non-radiative decay becomes problematic and all the emission is quenched [Lakowicz et al., 2002, Lakowicz et al., 2004, Stranik, 2007]. If the luminescent particle is placed beyond this quenching zone, the fluorescence enhancement should reach a maximum and then decrease as the distance increases [Stranik, 2007]. In this work, the spacing between the luminescent material and the Ag NPs will be manipulated by controlling the concentration of both luminescent material and the Ag NPs.

1.5.1 Materials

QDs used for this investigation were purchased from Cytodiagnostics, Canada. They were in solution (25 mg/ml in toluene solvent). They are Trilite nanocrystals (approximately 6 nm in size) with a CdSxSe1-x core encased in an inner shell of CdS and outer shell of ZnS. Two types of QDs with an emission peak at 490 nm and 450 nm were investigated they will be referred as QD-490 and QD-450. The QD-490 absorb light from 300 to 510 nm with one absorption peak at 472 nm and emit light between 450 to 550 nm. The QD-450 absorbs light from 300 to 425 nm with two absorption peaks at 360 and 430 nm. These QDs emit light

between 400 to 500 nm. Their LQY measured in PMMA film which was 58% for QD-490 and 34% for QD-450 [Ahmed, 2015].

A clear polymer poly(methyl methacrylate) (PMMA) (Carl Roth GmbH+Co.KG) was used for the encapsulation of pLDS layers. The MNPs used for the plasmonic interaction is silver (Ag). It was chosen because the SPR of the Ag particles is in the UV region (at 399 nm) which can be tuned in the synthesis process to match the absorption peaks of QDs. The materials used for the synthesis of Ag NPs were ascorbic acid (AA), trisodium citrate (TSC), polyvinylpyrrolidone (PVP) of M_w 10.000, distilled water passed through a Millipore system (ρ =18.2 Ωm) and dimethylformamide (DMF) solvent (density 0.944 g/ml at 20^{o}C, refractive index 1.43). The preparation of the Ag NPs followed the method reported by Ledwith et al., [2007] which produces highly stable shaped particles. It is based on the reduction of Ag ions by AA in the presence of citrate-stabilized Ag seed, additional TSC and the capping agent PVP. The colour of the solution is controlled by varying the concentration of the TSC [Ledwith et al., 2007, Ahmed et al., 2016a]. A TSC concentration of 0.006 (Ag NP1) and 0.011 mM (Ag NP2) were used to match the absorption peaks of QD-450 and QD-490 respectively. Ag NPs were synthesised in water followed by immediate centrifugation using an Avanti TM J-250-centrifuge at 8.133 rpm for 30 minutes and re-suspended in DMF. All chemicals for the synthesis were supplied by Sigma Aldrich.

SEM analysis revealed that spherical shapes are present in Ag NP 1 as presented in figure 11a. As for Ag NP 2 triangular and spherical shapes are present with triangular shapes being the dominant structures as seen in figure 11b [Ahmed et al., 2016a].

The peaks at 410 nm and at 335 nm are attributed to the presence of the spherical particles This result is consistent with what has been reported by [Ledwith et al., 2007] and also with the optical spectra results which also indicates that the synthesised Ag NP 2 are of triangular and spherical shapes [Krutyakov et al., 2008]. The particles were uniform in size distribution with an average diameter of 35 ± 5 nm for Ag NP 1 and 45 ±5 nm for Ag NP 2.

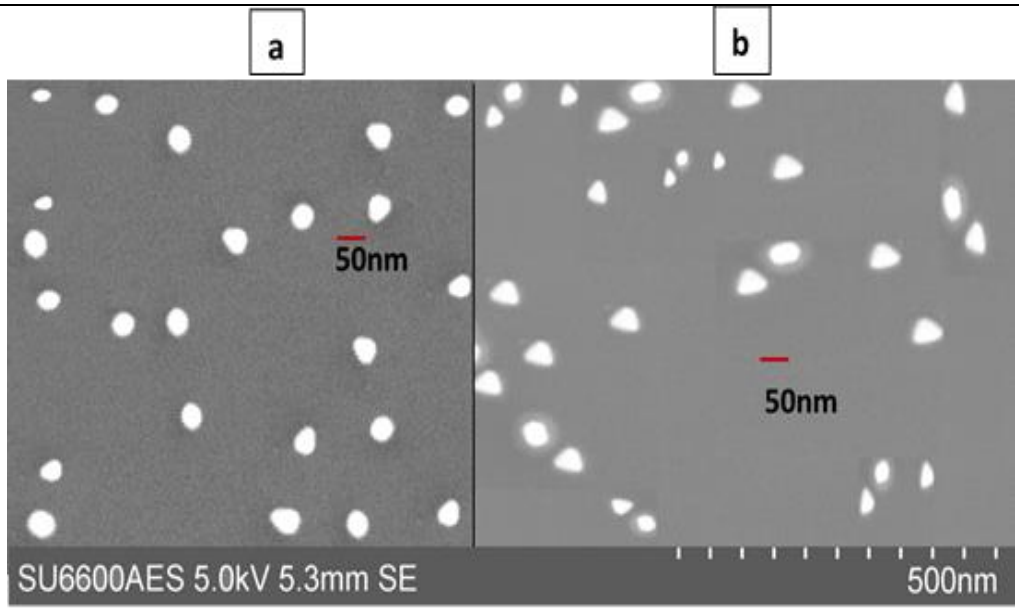

Figure 11: SEM images of synthesised Ag NPs a) Ag NP 1 and b) Ag NP 2. The average size of particles is 35 ± 5 nm for Ag NP 1 and 45 ± 5 nm for Ag NP 2.

1.5.2 Ag NPs in PMMA

Since the optical properties of the Ag NPs are dependent on the surrounding medium [Kelly et al., 2003, Xua et al., 2006] it was important to optimise Ag NPs properties in PMMA for pLDS layers. It is important that Ag NPs retain their optical properties in PMMA, i.e., their optical spectra for example should be similar to those in their solution (DFM). Ag NPs were re-suspended in DFM and dispersed in PMMA by simply adding Ag NPs in PMMA solution and magnetically stirring for 20 minutes followed by placing in an ultra-sonic bath for another 15 minutes. Prepared solutions were drop cast on glass substrates (size 4.5×2.5×1 mm) and cured for 72 hours at 25 ^{o}C and under a vacuum of 800 mbar. Uniform layers, as shown in figure 12, were obtained when removed from the glass substrates. The average thickness of the layers was measured by white light interferometer technique and found to be 0.95 ± 0.05 µm.

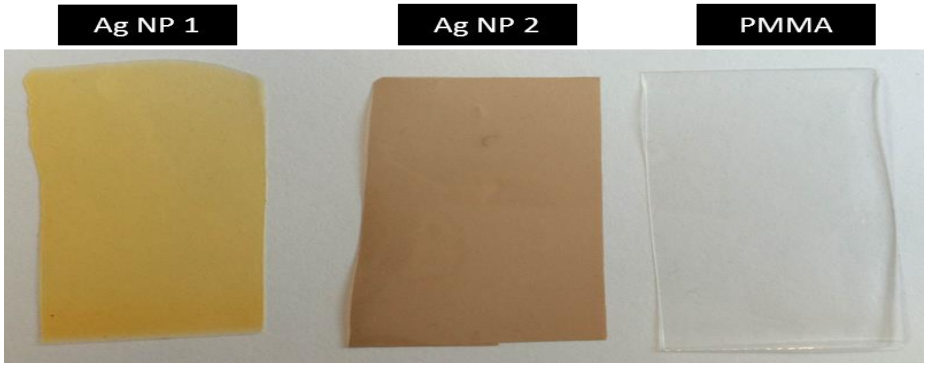

Figure 12: Ag NP 1, Ag NP 2 and blank PMMA layers prepared by drop -casting technique.

1.5.3 Optimisation of pLDS Composite Layers

The same process was undertaken for the pLDS composite layers, with the addition of previously optimized concentration for QD-490 at 0.09wt% and for QD-450 at 0.10wt% presented in figure 13 and figure 14 respectively. Higher than these concentrations the emission intensity starts to decrease. These optimized concentration were mixed with the Ag NPs and sonicated in an ultrasonic bath for 25 minutes before being added to the PMMA solution. The Ag NPs concentrations were varied from 0 to 50 ppm. (0 ppm refers to sample containing only QDs) Varying the concentration of the Ag NPs allowed the optimization of the maximum fluorescence enhancement of the QDs in the composite layers.

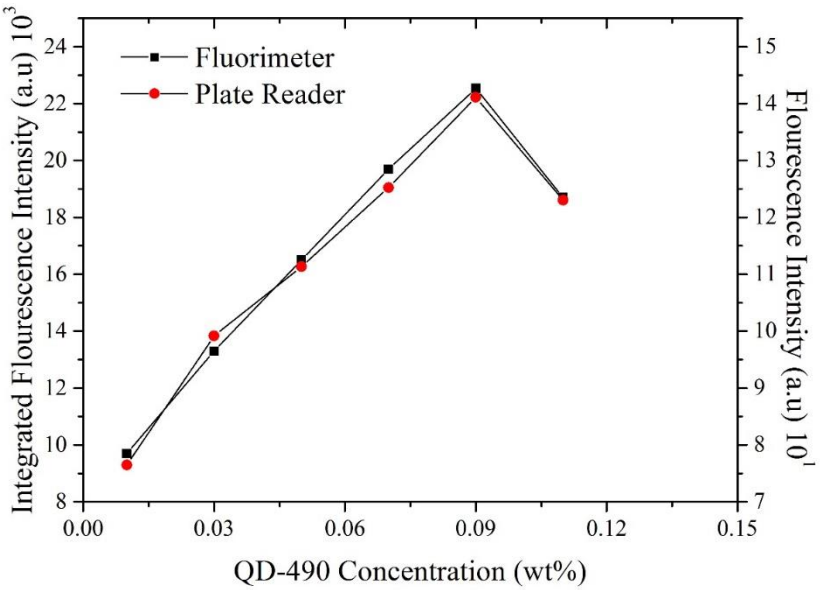

Figure 13: Integrated fluorescence spectra of QD-490 LDS layer as function of QD concentration, using fluorimeter and plate reader measurements.

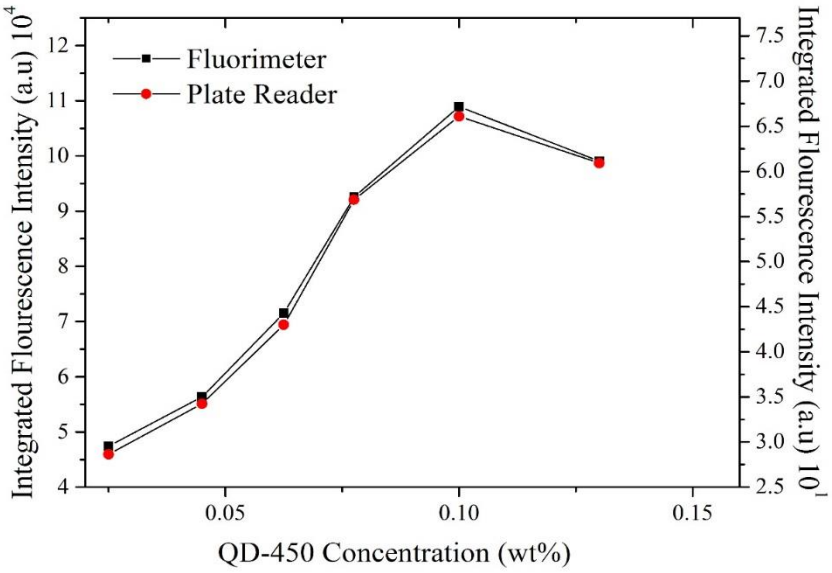

Figure 14: Integrated fluorescence spectra of QD-450 LDS layer as function of QD concentration, using fluorimeter and plate reader measurements.

1.5.4 Device Fabrication

CdTe mini-modules 15x 15 cm (Advanced Solar Power Inc, China), were used to assess the downshifting effect of pLDS composite layer of QD-490. The modules have an active area of 194 cm^2 after masking. Devices were fabricated by directly depositing the layers on top of the CdTe mini-modules surface, using PMMA solution to glue the layers. The deposited layers were left for three days to dry and stick to the cells as presented in figure 15. In order to determine the performance of the CdTe solar cells before and after downshifting layer encapsulation, the electrical characterization of a bare CdTe solar cell (figure 15a) was compared to CdTe solar cell encapsulated with LDS layer of QD-490 (figure 15b), and with pLDS composite layer of QD-490 (figure 15c).

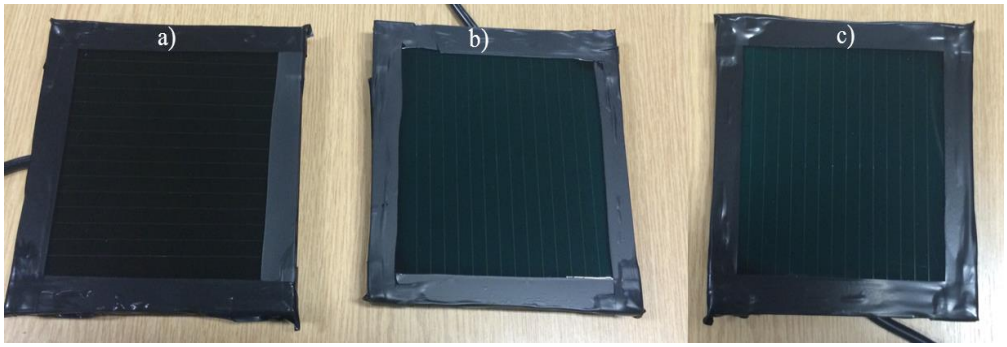

Figure 15: CdTe mini modules (15x 15cm). a) A clear modules, b) encapsulated with an LDS layer of QD-490 c) with pLDS composite layer of QD-490.

1.5.5 Characterization Techniques

Optical measurements

UV/Vis/NIR absorption spectroscopy was used to measure the absorption characteristics of the pLDS layers. UV/Vis/NIR absorption spectrometer used was a Perkin Elmer Lambda 900 using an integrating sphere configuration to minimize the effect of scattering losses due to the presence of Ag NPs. A blank PMMA sample was used as a reference during the measurements. The emission spectra of the LDS layers were measured by optically pumping samples using a monochromated light source using Luminescence spectrometer Perkin Elmer LS55B.

I–V measurements

Current-Voltage measurements were performed with a Keithley 2400 SMU (Source Meter Unit). The light source used was a metal halide discharge lamp (Griven, GR0262). An additional low intensity UV lamp (0.49 mW/cm2), is introduced so that spectral mismatch is minimized in the region 300-400 nm where the LDS material absorption is most significant. The percentage of spectral irradiance within six defined wavelength bands (300-1100 nm) according to the ASTMG173-03 standard and corresponding % values for the Griven light source with and without an additional UV lamp was reported [Ahmed et al., 2016a]. Five current – voltage measurements were taken for each device and results were averaged. The deviation between measurements was less than 3%.

External quantum efficiency (EQE) measurements

EQE system used was Bentham PVE300 of one sun (1000 w/m^2) during the measurements. The system uses a monochromatic probe source from a TMc300, 300 mm focal length monochromator, and a dual Xenon/quartz halogen light source providing optimum illumination from 300 to 1100 nm with uncertainties of 5 % for 300−400 nm. The monochromatic beam area is 1.85 mm^2 and is directed at the centre of the cell, measuring the photocurrent generated by the cell at each wavelength.

1.5.6 Results and Discussion

Figure 16 and 17 show UV/Vis extinction for Ag NP1 and Ag NP 2 in DMF and in PMMA layers, respectively. The extinction spectra have shown that Ag NP retain their properties during re-dispersion in PMMA and in the curing process. A red shift ~ 7 nm has been observed in the longitudinal SPR of both Ag NPs which is believed to be due to the refractive index difference in DMF 1.43 and in PMMA 1.48. SPR of Ag NP 1 has been shifted from 435 to 442 nm while SPR of Ag NP 2 was shifted from 477 to 484. SPR peaks in water were at 331 and 470 nm for Ag NP 1 and Ag NP 2, respectively, the red-shift observed is also attributed to the refractive index difference between water and DMF.

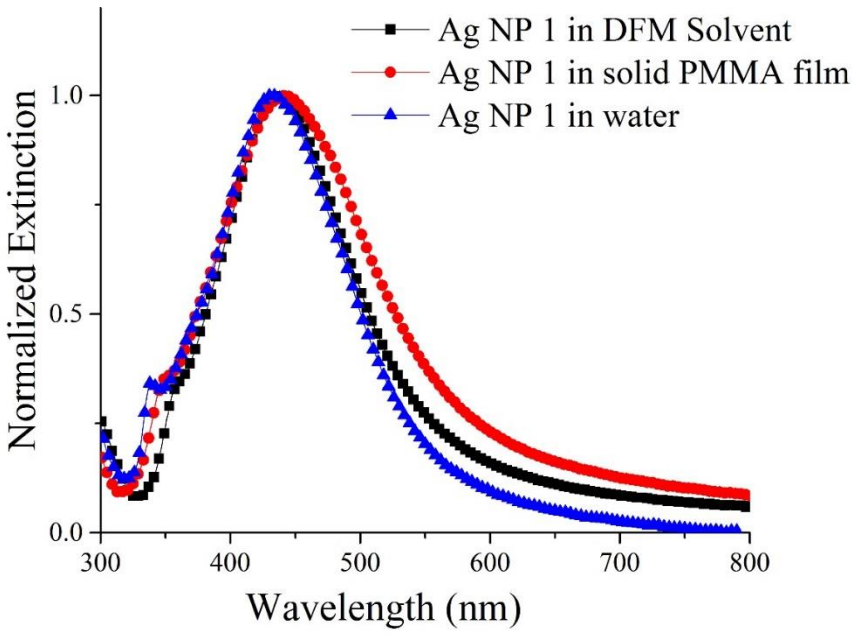

Figure 16: Normalized UV/Vis spectra of Ag NP 1 in DMF and in PMMA solid film and water.

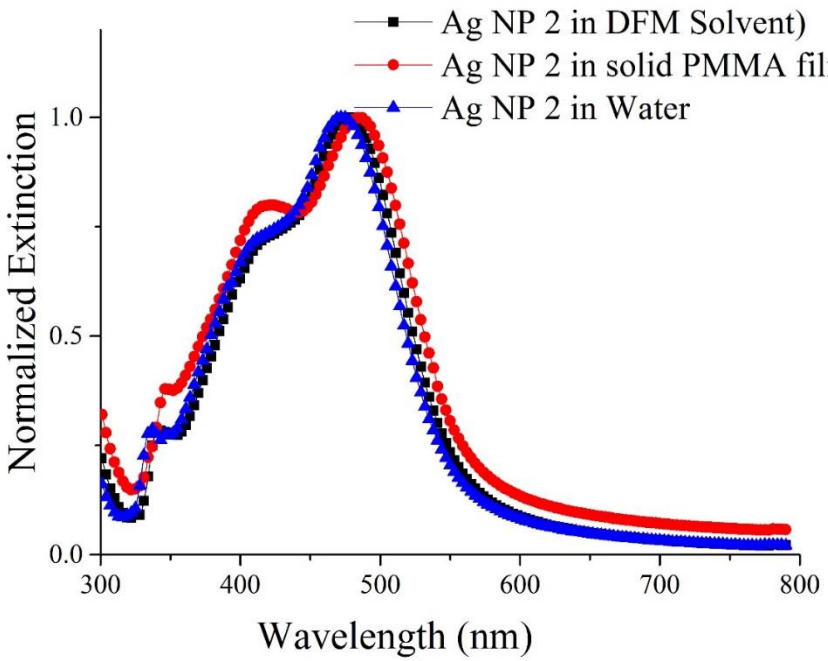

Figure 17: Normalized UV/Vis spectra of Ag NP 2 in DMF and in PMMA solid film and water.

Figure 18 shows the absorption measurements of the different pLDS composite layers of QD-450 prepared with different Ag NP 1 concentrations. It has been observed that absorption increased with increasing Ag NP 1 concentration. This enhancement strongly depends on the overlap between QD-450 absorption peak and Ag NP 1 extinction peak. The greater overlap leads to higher absorption [Stranik, 2007, Ahmed et al., 2016a]. This was also observed for pLDS composite layers of QD-490 presented in figure 19.

The enhancement observed can be attributed to the presence of the Ag NP 2 and can be explained by (i) SPR extinction in Ag NP increases their optical cross section which results in more light being provided to the QDs and lead to an increase in their absorption. (ii) Increased the optical pathlength of light in the composite layers by SPR of Ag NP. (iii) MNP exhibit strong scattering of incident light which greatly enhance the local electrical fields at the SPR resonance. When QDs fall within the enhanced zone their absorption is increased. The scattered light from Ag Np 1 and Ag NP 2 is interacting with QD-490 and QD-450 in the composite layer and increasing its radiative energy transition hence, the absorption.

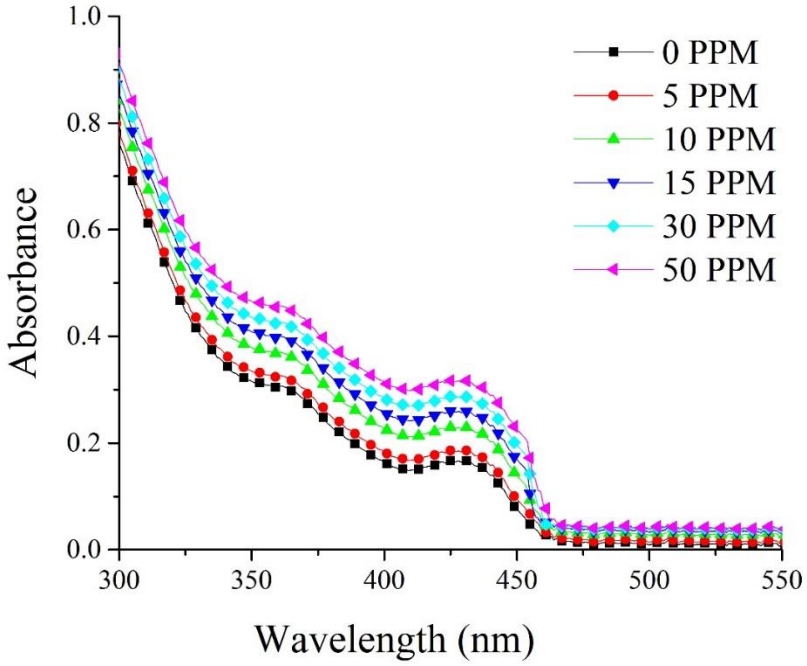

Figure 18: Absorbance spectra of pLDS of QD-450 layers with various Ag NP 1 concentrations.

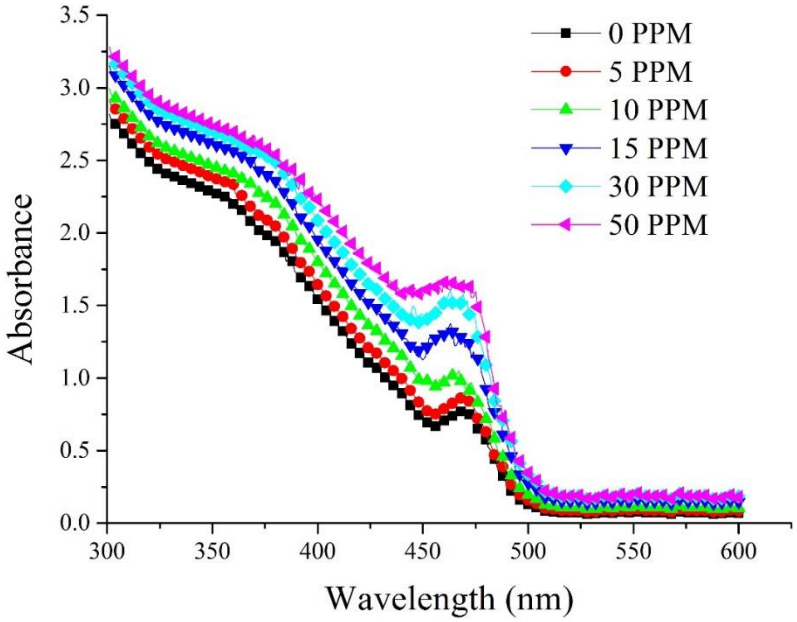

Figure 19: Absorbance spectra of pLDS of QD-490 layers with various Ag NP 2 concentrations.

The pLDS composite layers emission was characterised by fluorescent spectroscopy. Figure 20 shows the emission measurements of the pLDS composite layers for QD-450 where the excitation wavelength was at 380 nm. The enhancement was calculated as the difference between the emission spectrum with and without Ag NP. It can be seen that the fluorescence enhancement increases with increasing Ag NP 1 concentration, reaching a maximum at concentration of 10 ppm, and decreased thereafter. This was also observed for QD-490 with the excitation wavelength at 405 nm, presented in figure 21. The maximum enhancement was observed at a concentration of 15 ppm.

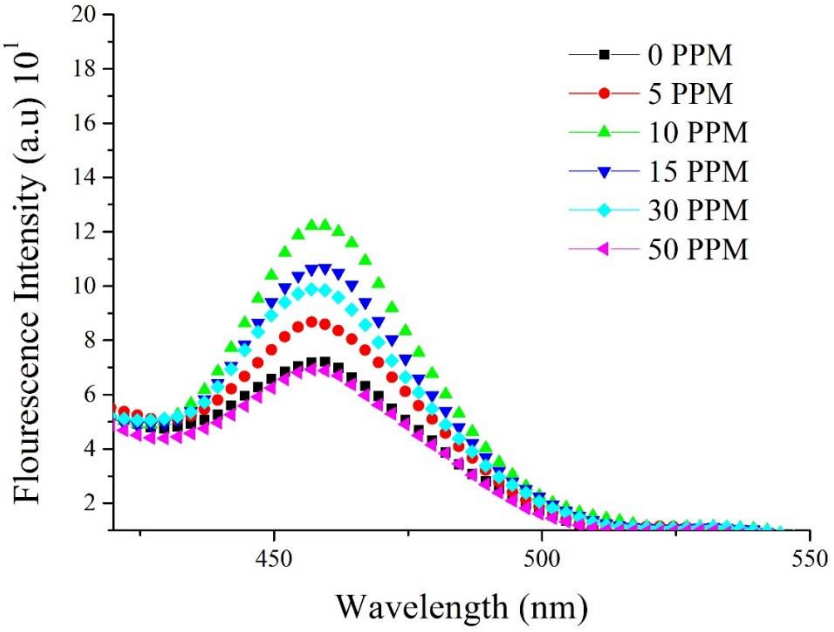

Figure 20: Emission spectra of pLDS composite layer of QD-450 with varying the Ag NP 1 concentrations.

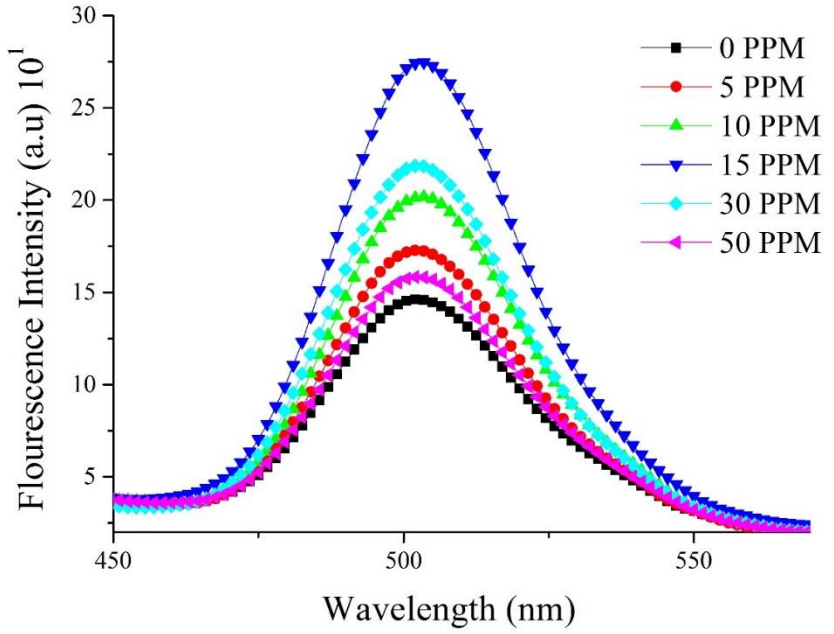

Figure 21: Emission spectra of pLDS composite layer of QD-490 with varying the Ag NP 2 concentrations.

Maximum fluorescence enhancement was significant for concentrations of 10 ppm and 15 ppm for QD-450 and QD-490, respectively. Enhancement was calculated for pLDS composite layers with different concentrations and presented in figures 22 and 23. Maximum enhancement was found to be 45% relative to the blank QD-450 LDS layer with no Ag NP and 60% for QD-490.

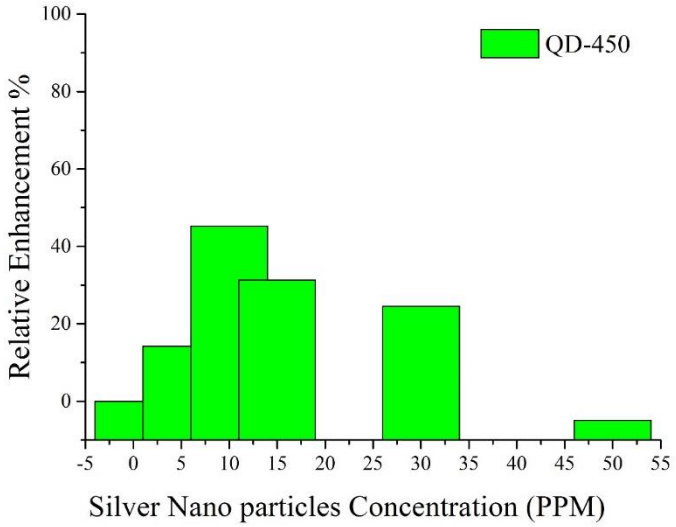

Figure 22: Relative fluorescence enhancement calculated for QD-450 with Ag NP 1 composite LDS layers, maximum enhancement observed for Ag NP 1 concentration of 10 ppm.

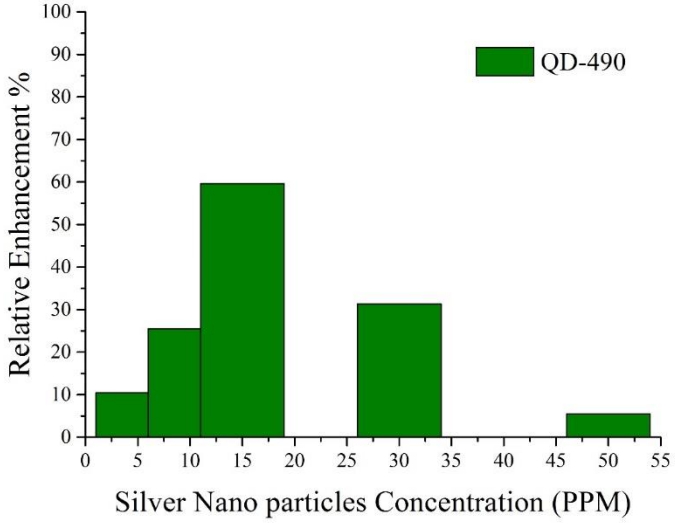

Figure 23: Relative fluorescence enhancement calculated for QD-490 with Ag NP 2 composite LDS layers, maximum enhancement observed for Ag NP 2 concentration of 10 ppm.

In general, these results can be explained as the overlap between the absorption peak of the luminescent materials and SPR frequency of Ag NP leading to the fluorescence emission enhancement. This is expected as the theoretical condition for enhanced fluorescence excitation is the overlap of the SPR with the absorption spectra of luminescent species [Lakowicz et al., 2002, Lakowicz et al., 2004]. At higher concentrations it is believed that a portion of luminescent material particles is in the non-radiative zone which led to emission quenching by non-radiative energy transfer from the luminescent particles to Ag NP. If the luminescent particle is placed beyond this quenching zone, the fluorescence enhancement should reach a maximum (at the optimum distance) and then decrease as the distance increases [Stranik, 2007, Chandra, 2013].

Figure 24 show the JV curves for CdTe mini modules under Griven GR062 lamp illumination for LDS QDs layers. The mini modules were under illumination for 60 seconds before taking measurements in order to ensure a uniform solar simulator illumination on the cells due to their size. The increase in the current generation for the plasmonic layer is clearly visible compared to LDS layer of only QD-490 and to the reference CdTe cell. J-V characteristics for CdTe mini modules with and without pLDS layers are presented in table 2.

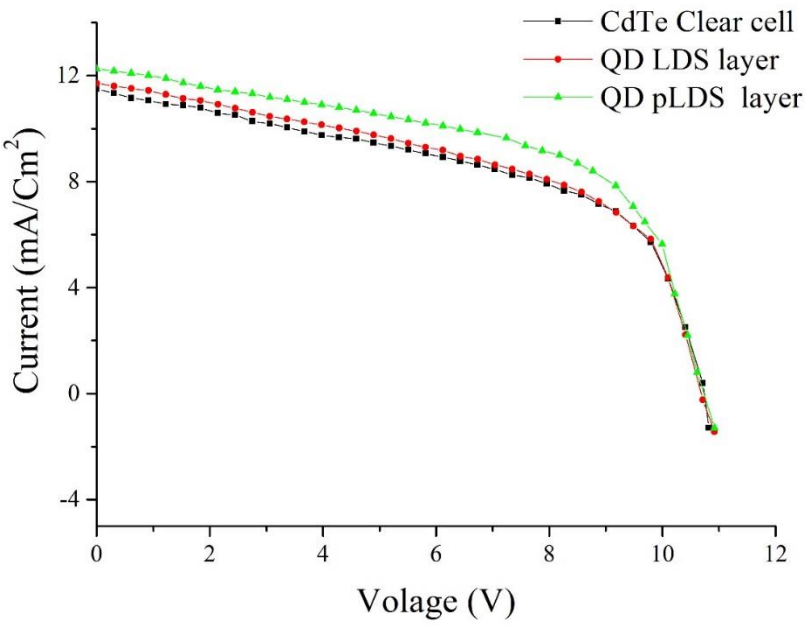

Figure 24: JV curves of CdTe mini modules with (i) no LDS layer, (ii) with QD-490 LDS layer and (iii) with pLDS composite layer of QD-490.

Table 2: Measured IV characteristic of CdTe mini modules under Griven GR0262 lamp solar simulator with LDS layer and pLDS composite layer of QD-490

	J_{sc} mA/cm^2	V_{oc} (Volts)	FF	η %	ΔJsc % ±0.03
CdTe (reference)	11.5	10.9	0.52	5.3	-
LDS	11.7	10.9	0.54	5.4	1.7
pLDS	12.2	11.00	0.55	6.0	6.1

The electrical characterization showed an increase of 1.7% in the current density due to the presence of QDs when compared to the bare CdTe mini modules. An enhancement of 6.1% was calculated for the pLDS composite layer of QD-490. There is a 6.1% increase in the current density for pLDS composite layer when compared with the LDS layer. The differences observed in the short circuit current can be explained by the enhancement due to the presence of the Ag NPs in the composite layer.

Figure 25 shows the EQE measurements measured for the CdTe mini-modules. As can be observed the EQE of the reference CdTe solar cell has a poor optical response and hence low EQE at wavelengths below 400 nm.

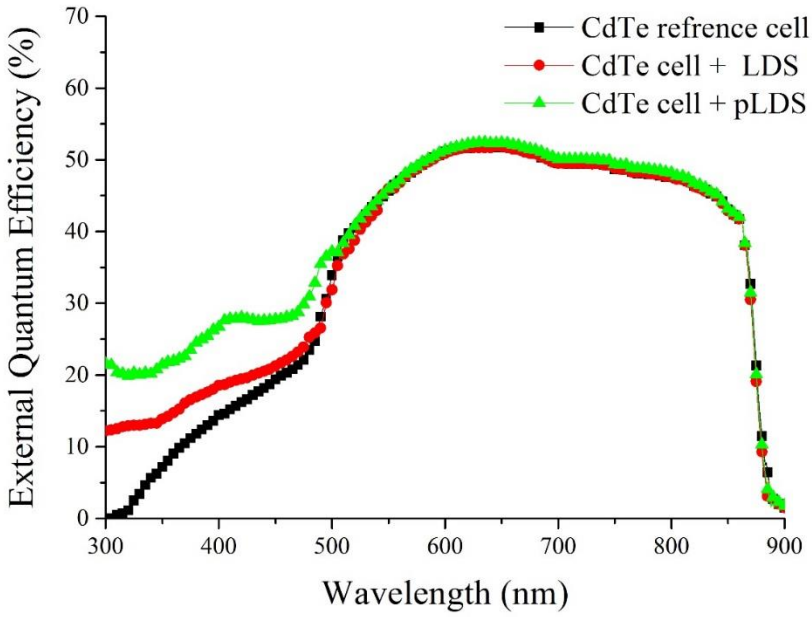

Figure 25: EQE spectrum of CdTe mini-modules with no (i) LDS layer, (ii) with LDS layer and (iii) with pLDS composite layer of QD-490.

At these wavelengths, EQE is enhanced for the cell encapsulated with QDs LDS layer reaching 12 – 25% between 300-485 nm. There is a slight reduction at 485-505 nm due to the overlap between the absorption and emission spectra which causes self-absorption. This effect is due to the relative difference in EQE between the QDs absorption and emission wavelengths which is not great enough to overcome the loss associated with reabsorption in these regions [Ross et al., 2012]. This reduction however is offset in the plasmonic layer which shows a significant increase of 20-35% between 300-485 nm. This is attributed to the presence of Ag NP in the composite layer enhancing QDs absorption and emission and therefore enhancing the EQE curve at a short wavelengths.

The gain in current density (J_{sc}) from LDS layers demonstrated from EQE measurement is compared with the theoretical analysis as follows;

$$\boldsymbol{J_{Sc} = q \int_{\lambda_1}^{\lambda_2} \varphi(\lambda) EQE(\lambda) d\lambda} \qquad \text{Equation 13}$$

where q is the electron charge**,** φ is the photon flux λ_1 and λ_2 define the range of the spectrum for which J_{sc} is to be calculated.

J_{sc} was calculated from Griven GR0262 lamp solar simulator and from AM1.5G ASTM standard and presented in table 3. There are two wavelength regions where J_{sc} was calculated at 300-500 nm, where the QDs is absorbing and the action of the LDS layer is more significant and at 300-1100 nm to see the overall effect of LDS layer for which the solar cells response. J_{sc} calculated for CdTe solar cell from the EQE measurements in table 3 was found to be in good agreement with J_{sc} measured in table 2 and the difference is within the experimental error of the EQE measurements of ±0.05%. J_{sc} calculated for the AM1.5G ASTM standard was found to be higher compared to Griven solar simulation which is due to the spectrum mismatch between lamps [Ahmed et al., 2016a]. The results discussed here are for Griven solar simulation however, the results obtained from the AM1.5G calculations confirm the same trend.

Significant increase at 300–500 nm was calculated for the J_{sc} reaching 60% for composite pLDS layer and 20% for the QD-LDS compared to reference CdTe solar cell. The composite pLDS layer showed an increase of 33.3% in the J_{sc} compared to the LDS layer. This behaviour is due to the plasmonic interaction of Ag NP enhancing the QDs optical properties and hence increasing the photo current generated by the CdTe solar cell.

At wavelengths 300-900 nm, LDS layer showed an increase of only 1.7% in current density compared to the bare reference CdTe solar cell while an enhancement up 6 % was calculated for the pLDS composite layer. An increase of 5.9% in current density was calculated for the pLDS layer when compared with the LDS layer. These results is following the same trend which has been reported for the same plasmonic LDS layer fabricated for c-Si and DSSC devices [Ahmed, et al., 2016a].

Table.3: Calculated J_{sc} of the CdTe mini-module from the integration of the EQE curves combined with (a) Griven GR062 lamp solar simulator and (b) AM1.5G ASTM standard photon flux density with LDS layers

(a) J_{sc} calculated from Griven GR0262 lamp solar simultaor				
	J_{sc} (mA/cm^2) 300-500 nm	ΔJ_{sc} ± 0.05% 300-500 nm	J_{sc} (mA/cm^2) 300-900 nm	ΔJ_{sc}± 0.05% 300-900 nm
CdTe reference	1.0	-	11.7	-
LDS	1.2	20	11.9	1.7
pLDS	1.6	60	12.4	6.0
(b) J_{sc} calculated from AM1.5G ASTM standard				
	J_{sc} (mA/cm^2) 300-500 nm	ΔJ_{sc} ± 0.05% 300-500 nm	J_{sc} (mA/cm^2) 300-900 nm	ΔJ_{sc}± 0.05% 300-900 nm
CdTe reference	1.2		12.6	
LDS	1.4	27.3	13.0	3.2
pLDS	1.8	63.6	13.5	7.1

CONCLUSION

This work has presented plasmonic down shifting layers (pLDS) for CdTe mini-modules devises. Composite layers were successfully fabricated by drop casting on glass substrates with varying Ag NPs concentration from 0 to 50 ppm while fixing QDs concentrations to previously determined optimum concentrations. This allowed the manipulation of spacing between the Ag NPs and the QDs particles. The presence of silver nanoparticles produced a plasmonic interaction that has significantly improved the absorption and emission of QDs. A 60 % relative increase in the emission intensity was calculated for QD-490 at Ag NPs concentration of 15 ppm [Ahmed at el., 2016a] while an increase of 45% was measured for QD-450 at Ag NP concentration of 10 ppm. These enhancements of the emission are promising for the enhancement of the performance of PV devices utilizing luminescent downshifting layers.

Plasmonic LDS layers have shown to improve the J_{sc} of CdTe mini-modules devices reaching ~ 60% at short wavelengths 300-500 nm demonstrating the possible improvement due to the action of plasmonic LDS layers. Results from both J–V and EQE measurements confirm this improvement. Plasmonic interaction therefore opens up the use of many types of

lumophores that have previously been rejected for inclusion in LDS layers because of their low quantum yield and low absorption coefficient.

Acknowledgements

The authors would like to acknowledge funding from the Irish Higher Education Authority under the Strand 3 program (SEAR Project) and European Research Council– Brussels – Belgium (PEDAL Project Number 639760). The authors also acknowledge the FOCAS Institute for use of equipment and facilities at the Dublin Institute of Technology.

Authors gratefully acknowledge helpful assistance of Dr. Subhash Chandra. Also thanks to Dr. Donagh O'Mahony and Dr. Richard Winfield for allowing us to use their Bentham PVE300 facility at Tyndall National Institute as well for their assistance and helpful discussion.

REFERENCES

Aboueiezz, M., and Waters, P. F., 1978. Studies on the Photodegradatoin of Poly(Methyl Methacrylate). *US Department of Commerce, National Engineering Lab (NBS)*, Washington, USA, 1-55.

Ahmed, 2015. Materials Characterization and Plasmonic Interaction in Enhanced Luminescent Down-Shifting Layers for Photovoltaic Devices. PhD thesis, Dublin Institute of Technology, Ireland.

Ahmed, H., Doran, J., and McCormack, S., 2016a. Increased Short-Circuit Current Density and External Quantum Efficiency of Silicon and Dye Sensitised Solar Cells through Plasmonic Luminescent Down-Shifting Layers. *Solar Energy*, **126**, 146–155.

Ahmed, H., Kennedy, M., Doran, J., McCormack, S. J., Galindo, S., Voz, C., and Puigdollers, J., 2012a. Lumogen Violet Dye as Luminescent Down-Shifting Layer for c-Silicon Solar Cells. *In Proceedings of the 27th European Photovoltaic Solar Energy Conference and Exhibition*, Frankfurt, Germany.

Ahmed, H., Kennedy, M., Doran, J., McCormack, S. J., Pirriera, M. D., Gutierrez-Tauste, D., and Aubouy, L., 2012b. Characterization of Luminescent Down-Shifting Materials and Applications for Enhanced Photovoltaic Devices. *In Proceedings of the 8th Photovoltaic Science Application and Technology (PVSAT-8) Conference and Exhibition*, Northumbria University, UK.

Ahmed, H., McCormack, S. J., and J. Doran, 2016b. External Quantum Efficiency Improvement with Luminescent Downshifting Layers: Experimental and Modelling. *International Journal of Spectroscopy*, 2016, Article ID 8543475, 1-7.

Al-Azawi, M. A., Bidin, N., Bououdina, M., and Mohammad, S.M., 2016. Preparation of Gold and Gold–Silver alloy Nanoparticles for Enhancement of Plasmonic Dye-Sensitized Solar Cells Performance. *Solar Energy*, **126**, 93-104.

Alonso-Álvarez, D., Ross, D., Klampaftis, E., McIntosh, K. R., Jia, S., Storiz, P., Stolz, T., and Richards, B. S., 2014. Luminescent Down-Shifting Experiment and Modelling with Multiple Photovoltaic Technologies. *Progress in Photovoltaics: Research and Applications*, **23**, 479-497.

Andrew, P., and Barnes, W. L., 2000. Förster Energy Transfer in an Optical Microcavity. *Science*, **290**, 785–788.

Andrew, P., and Barnes, W. L., 2004. Energy Transfer across a Metal Film Mediated by Surface Plasmon Polaritons. *Science*, **306**, 1002–1005.

Anger, P., Bharadwaj, P., and Novotny, L., 2006. Enhancement and Quenching of Single-Molecule Fluorescence. *Physical Review Letters*, **96**, 113002.

Angrist, S. W., *Direct Energy Conversion (Series in Mechanical Engineering & Applied Mechanics)*, Allyn & Bacon: Boston, 1982; 4th edition, 1-468.

Aslan, K., Lakowicz, J. R., Szmacinski, H., and Geddes, C. D., 2004. Metal-Enhanced Fluorescence Solution-Based Sensing Platform. *Journal of Fluorescence*, **14**, 677-679.

Aslan, K., Lakowicz, J. R., Szmacinski, H., and Geddes, C. D., 2005. Enhanced Ratiometric pH Sensing Using SNAFL-2 on Silver Island Films: Metal-Enhances Fluorescence Sensing. *Journal of Fluorescence*, **15**, 37-39.

Bagnall, D. M., and Boreland, M., 2008. Photovoltaic Technologies. *Energy Policy*, **36**, 4390-4396.

Bakker, B. H., Goes, M., Hoebe, N., van Ramesdonk, H. J., Verhoeven, J. W., Werts, M. H., Hofstraat, J. W., 2000. Luminescent Materials and Devices: Lanthanide Azatriphenylene Complexes and Electroluminescent Charge Transfer Systems. *Coordination Chemistry Reviews*, **208**, 3–16.

Becquerel, E., 1840. *Traite experimental de l'electricite et du magnetisme*. Imperimerie Royale, Paris, France. *Trafficking of Experimental Electricity and Magnetism*, Royal printing Paris, France.

Bedair, S. M., Lamorte, M. F., and Hauser, J. R., 1979. A Two-Junction Cascade Solar-Cell Structure. *Applied Physics Letter*, **34**, 38–39.

Bella, F., Griffini, G., Gerosa, M., Turri, S., and Bongiovanni, R., 2015. Performance and Stability Improvements for Dye-Sensitized Solar Cells in the Presence of Luminescent Coatings. *Journal of Power Sources*, **283**, 195-203.

Benanti, T. L., and Venkataraman, D., 2006. Organic solar cells: An overview: Focusing on Active Layer Morphology. *Photosynthesis Research*, **87**, 73–81.

Bentham Ltd, 2104. Technical Note: Spectral Characterisation of Photovoltaic Devices. *Available Online* at http://www.bentham.co.uk/pdf/PV_Technical_Note.pdf. Last accessed 12/8/2016.

Binnemans, K., 2009. Lanthanide-Based Luminescent Hybrid Materials. *Chemistry Review*, **109**, 4283–4374.

Bohren, C. F., and Huffman, D. R. *Absorption and Scattering of Light by Small Particles*. John Wiley & Sons, New York, USA, 1983; Chapter 11, 12, P 282.

Boland, P., Lee, K., Dean, J., and Namkoong, G., 2010. Design of Organic Tandem Solar Cells Using Low- and High-Bandgap Polymer: Fullerene Composites. *Solar Energy Materials & Solar Cells*, **94**, 2170–2175.

Bruchez Jr, M., Moronne, M., Gin, P., Weiss, S., and Alivisatos. A. P., 1998. Semiconductor Nanocrystals as Fluorescent Biological Labels. *Science*, **281**, 2013-2016.

Calander, N., and Willander, M., 2002. Theory of Surface-Plasmon Resonance Optical-Field Enhancement at Prolate Spheroids. *Journal of Applied Physics*, **97**, 4878-4884.

Catchpole, K. R., and Pillai, S., 2006. Surface Plasmons for Enhanced Silicon Light-Emitting Diodes and Solar Cells. *Journal of Luminescence*, **121**, 315–318.

Catchpole, K. R., and Polman, A., 2008. Plasmonic Solar Cells. *Optics Express*, **16**, 21793-21799.

Chan, G. H., Zhao, J., Hicks, E. M., Schatz, G. C., and Van Duyne, R. P., 2007. Plasmonic Properties of Copper Nanoparticles Fabricated by Nanosphere Lithography. *Nano Letters*, **7**, 1947-1952.

Chan, G. H., Zhao, J., Schatz, G. C., and Van Duyne, R. P., 2008. Localized Surface Plasmon Resonance Spectroscopy of Triangular Aluminum Nanoparticles. *The Journal of Physical Chemistry C*, **112**, 13958–13963.

Chander, N., Sardana, S. K., Parashar, P. K., Khan, A. F., Chawla, S., and Komarala, V. K., 2015. Improving the Short-Wavelength Spectral Response of Silicon Solar Cells by Spray Deposition of YbVO4: Eu3+ Downshifting Phosphor Nanoparticles. *IEEE Journal of Photovoltaics*, **5**, 1373-1379.

Chandra, S., 2013. Approach to Plasmonic Luminescent Solar Concentration. PhD thesis, Dublin Institute of Technology, Ireland.

Chandra, S., McCormack, S. J., Doran J., Kennedy, M., and Chatten, A. J., 2010. New Concept for Luminescent Solar Concentrator. *In Proceedings of the 25th European Photovoltaic Solar Energy Conference*, Valencia, Spain, September, 759-762.

Chandra, S., McCormack, S. J., Doran J., Kennedy, M., and Chatten, A. J., 2012. Enhanced Quantum Dot Emission for Luminescent Solar Concentrators Using Plasmonic Interaction. *Journal of Solar Energy Materials & Solar Cells*, **98**, 385-390.

Chatten, A. J., Barnham, K. W., Buxton, B. F., Ekins-Daukes, N. J., and Malik, M. A., 2003. A New Approach to Modelling Quantum Dot Concentrators. *Solar Energy Materials & Solar Cells*, **75**, 363–371.

Chen, O., Zhao, J., Chauhan, V.P., Cui, J., Wong, C., Harris, D.K., Wei, H., Han, H.S., Fukumura, D., Jain, R.K. and Bawendi, M.G., 2013. Compact High-Quality CdSe–CdS Core–Shell Nanocrystals with Narrow Emission Linewidths and Suppressed Blinking. *Nature materials*, **12**, 45-451.

Chen, S. F., Cheng, F., Mei, Y., Peng, B., Kong, M., Hao, J. Y., Zhang, R., Xiong, Q. H., Wang, L. H., and Huang, W., 2014. Plasmon-Enhanced Polymer Photovoltaic Cells Based on Large Aspect Ratio Gold Nanorods and the Related Working Mechanism. *Applied Physics Letters*, **104**, 213903.

Cheng, Z., Su, F., Pan, L., Cao, M., and Sun, Z., 2010. CdS Quantum Qot-Embedded Silica Film as Luminescent Down-Shifting Layer for Crystalline Si Solar Cells. *Journal of Alloys and Compounds*, **494**, L7–L10.

Cho, C.Y., Hong, S. H. and Park, S. J., 2015. Improvement of Optical and Electrical Properties of Indium Tin Oxide Layer of GaN-Based Light-Emitting Diode by Surface Plasmon in Silver Nanoparticles. *Thin Solid Films*, **590**, 76-79.

Chuanhao, L., Liangping, X., Hongtao, G., Ruiying, S., Chen, S., Haofei, S., and Chunlei, D., 2012. Broadband absorption enhancement in a-Si:H film solar cells sandwiched by pyramidal nanostructured arrays. Optical Express 20, A589.

Creighton, J. A., Blatchford, C. G., and Albrecht, M. G., 1979. Plasma Resonance Enhancement of Raman Scattering by Pyridine Adsorbed on Silver or Gold Sol Particles of Size Comparable to the Excitation Wavelength. *Journal of Chemical Society Faraday Transection 2*, **75**, 790–798.

Cui, H., Liu, X., Liu, F., Hao, X., Song, N., and Yan, C., 2014. Boosting Cu2ZnSnS4 Solar Cells Efficiency by a Thin Ag Intermediate Layer between Absorber and Back Contact. *Applied Physics Letters*, **104**, 041115.

Cuony. P., 2011. Optical Layers for Thin-film Silicon Solar Cells. PhD Thesis, École Polytechnique Fédérale de Lausanne, Switzerland.

Daghestani, H. N., and Day, B. W., 2010**.** Theory and Applications of Surface Plasmon Resonance, Resonant Mirror, Resonant Waveguide Grating, and Dual Polarization Interferometry Biosensors. *Sensors*, **10**, 9630-9646.

Daram, B., Al-Rawi, K. R., and Alshaikh Husssin, S. H., 2011. Improve the Performance Efficiency of Solar Cell by Using Epoxy Plates Doped with Rhodamine 6G Dye. *Indian Journal of Science and Technology*, **4**, 1726-1730.

De Mello Donegá, C., Hickey, S. G., Wuister, S. F., Vanmaekelbergh, D., and Meijerink, A., 2003. Single-Step Synthesis to Control the Photoluminescence Quantum Yield and Size Dispersion of CdSe Nanocrystals. *Journal of Physical Chemistry B*, **107**, 489-496.

Debije, M. G., Broer, D. J., and Bastiaansen, C. W., 2007. Effect of Dye Alignment on the Output of a Luminescent Solar Concentrator. *In Proceedings of the 22nd European Photovoltaic Solar Energy Conference and Exhibition*, Milan, Italy, 87-89.

Debije, M. G., Teunissen, J. P., Kastelijn, M. J., Verbunt, P. P., and Bastiaansen, C. W., 2009. The Effect of a Scattering Layer on the Edge Output of a Luminescent Solar Concentrator. *Solar Energy Materials and Solar Cells*, **93**, 1345-1350.

Debije, M. G., Verbunt, P. P. C., Rowan, B. C., Richards, B. S., and Hoeks, T. L., 2008. Measured Surface Loss From Luminescent Solar Concentrator Waveguides. *Applied Optics*, **47**, 6763-6768.

Di Lorenzo, M. L., Cocca, M., Avella, M., Gentile, G., Gutierrez, D., Della Pirriera, M., Torralba-Calleja, E., Kennedy, M., Ahmed, H., and Doran, J., 2016. Down Shifting in Poly(vinyl alcohol) Gels Doped with Terbium Complex. *Journal of Colloid and Interface Science*, **477**, 34-39.

Drury, E., Margolis, R., Denholm, P., Goodrich, A.C., Heath, G., Mai, T., Tegen, S. 2012. Solar Energy Technologies, Chapter 10. National Renewable Energy Laboratory. Renewable Electricity Futures Study, Vol. 2, Golden, CO: National Renewable Energy Laboratory, 1– 60.

Du, H., Chen, C., Krishnan, R., Krauss, T. D., Harbold, J. M., Wise, F. W., Thomas, M. G., and Silcox, J., 2002. Optical Properties of Colloidal PbSe Nanocrystals. *Nano Letters*, **2**, 1321-1324.

Duche, D., Torchio, P., Escoubas, L., Monestier, F., Simon, J., Flory, F., and Mathian, G., 2009. Improving Light Absorption in Organic Solar Cells by Plasmonic Contribution. *Solar Energy Materials & Solar Cells*, **93**, 1377–1382.

Dunbar, R. B., Pfadler, T., and Schmidt-Mende, L., 2012. Highly Absorbing Solar Cells—a Survey of Plasmonic Nanostructures. *Optical Express*, **20**, A177-A189.

Earp, A. A., Rawling, T., Franklin, J. B., and Smith, G. B., 2010. Perylene Dye Photodegradation Due to Ketones and Singlet Oxygen. *Dyes and Pigments*, **84**, 59–61.

Earp, A. A., Smith, G. B., Franklin, J., and Swift, P., 2004b. Optimisation of A three-Color Luminescent Solar Concentrator Daylighting System. *Solar Energy Materials & Solar Cells*, **84**, 411-426.

Earp, A. A., Smith, G. B., Swift, P. D., and Franklin, J., 2004a. Maximising the Light Output of A luminescent Solar Concentrator. *Solar Energy*, **76**, 655-66.

Ekins-Daukes, N. J., Adams, J., Ballard, I. M., Barnham, K. W. J., Browne, B., Connolly, J. P., Tibbits, T., Hill, G., and Roberts, J. S., 2009. Physics of Quantum Well Solar Cells. *In Proceeding of Society of Photographic Instrumentation Engineers Conference (SPIE)*, **7211**, 72110L1.-72110L11.

El-Sayed, M. A., 2001. Some Interesting Properties of Metals Confined in Time and Nanometer Space of Different Shapes. *Accounts of Chemical Research*, **34**, 257–264.

Enderlein, J., 2001, Theoretical Study of Single Molecule Fluorescence in a Metallic Nanocavity. *Applied Physics Letters*, **80**, 315-317.

EPHOCELL Project, 2013. Smart Light Collecting System for the Efficiency Enhancement of Solar Cells, *Available Online at* http://ipo.leitat.org/ephocell/. Last accessed 12/08/2016.

Escoubas, L., Simon, J. J., Torchio, P., Duché, D., Vedraine, S., Vervisch, W., Le Rouzo, J., Flory, F., Rivière, G., Yeabiyo, G., and Derbal, H., 2011. Bringing Some Photonic Structures for Solar Cells to the Fore. *Applied Optics*, **50**, C329-C339.

Ethayaraja, M., Ravikumar, C., Muthukumaran, D., Dutta, K., and Bandyopadhyaya, R., 2007. CdS-ZnS Core-Shell Nanoparticle Formation: Experiment, Mechanism, and Simulation. *The Journal of Physical Chemistry C*, **111**, 3246-3252.

ETSAP and IRENA, 2013. Solar Photovoltaic, *Technology Brief E11, Available Online* at www.etsap.org – www.irena.org. Last accessed 12/08/2016.

EurObserv'ER, 2014. Photovoltaic Barometer, *Available Online* at http://www.eurobserv-er.org/photovoltaic-barometer-2014/. Last accessed 12/08/2016.

EurObserv'ER, 2016. Photovoltaic Barometer, *Available Online* at http://www.eurobserv-er.org/photovoltaic-barometer-2016/. Last accessed 12/08/2016.

Eustis, S., and El-Sayed, M. A., 2006. Why Gold Nanoparticles are More Precious than Pretty Gold: Noble Metal Surface Plasmon Resonance and its Enhancement of the Radiative and Nonradiative Properties of Nanocrystals of Different Shapes. *Chemical Society Reviews*, **35**, 209–217.

Farahani, J. N., Pohl, D. W., Eisler, H. J., and Hecht, B., 2005. Single Quantum Dot Coupled to a Scanning Optical Antenna: A Tunable Superemitter. *Physical Review Letters*, **95**, 017402.

Faulkner, S., Carrie, M.-C., Pope, S. J. A., Squire, J., Beeby, A., and Sammes, P. G., 2004. Pyrene-Sensitised Near-IR Luminescence from Ytterbium and Neodymium Complexes. *Dalton Transactions*, **7**, 1405-1409.

Ferry, V. E., Munday, J. N., and Atwater, H. A., 2010. Design Considerations for Plasmonic Photovoltaics. *Advanced Materials*, **22**, 4794–4808.

Ford, G. W., and Weber, W. H., 1984. Electromagnetic Interactions of Molecules with Metal Surfaces. *Physics Reports*, **113**, 195-287.

Fort, E., and Gŕesillon, S., 2008. Surface Enhanced Fluorescence. *Journal of Physics D: Applied Physics*, **41**, 013001-013031.

Fraunhofer ISE, 2009. Annual Report. High Efficiency Multipl Solar Cells of III-V Semiconductors. Freiburg. Germany. *Available Online* at https://www.ise.fraunhofer.de/en/publications/veroeffentlichungen-pdf-dateien-en/infomaterial/annual-reports/Fraunhofer-ISE-Annual-Report-2009.pdf. Last accessed 12/08/2016.

Fraunhofer ISE, 2016. Photovoltaics Report. Freiburg. Germany. *Available Online* at www.ise.fraunhofer.dehttps://www.ise.fraunhofer.de/de/downloads/pdf-files/aktuelles/photovoltaics-report-in-englischer-sprache.pdf. Last accessed 12/08/2016.

Gallagher, S. J., Rowan, B. C., Doran, J., and Norton, B., 2007. Quantum Dot Solar Concentrator*:* Device Optimisation Using Spectroscopic Techniques. *Solar Energy*, **81**, 540–547.

Gaponenko, S. V., 1998. Optical of Semiconductor Nanocrystals. *Cambridge University Press*, UK.

Ghosh, S. K., and Pal, T., 2007. Interparticle Coupling Effect on the Surface Plasmon Resonance of Gold Nanoparticles: From Theory to Applications. *Chemical Review*, **107**, 4797-4862.

Glaeser, G. C., and Rau, U., 2007. Improvement of Photon Collection in Cu(In,Ga)Se_2 Solar Cells and Modules by Fluorescent Frequency Conversion. *Thin Solid Films*, **515**, 5964-5967.

Goetzberger, A., and Greubel, W., 1977. Solar Energy Conversion with Fluorescent Collectors. *Applied Physics*, **14**, 123–139.

Goetzberger, A., Knobloch, J., and Voss, B. *Crystalline Silicon Solar Cells*. John Wiley & Sons, New York, USA, 1998; Chapter 9, P 201.

Goldschmidt, J. C., Peters, M., Bösch, A., Helmers, H., Dimroth, F., Glunz, S. W., and Willeke, G., 2009. Increasing the Efficiency of Fluorescent Concentrator Systems. *Solar Energy Materials & Solar Cells*, **93**, 176-182.

Grätzel, M., 2003. Dye-Sensitized Solar Cells: Review. *Journal of Photochemistry and Photobiology C: Photochemistry Reviews*, **4**, 145-153.

Green, M. *Third Generation Photovoltaic: Advanced Solar Energy Conversion*. Springer, Berlin, Germany. 2006.

Green, M., 2002. Third Generation Photovoltaic Solar Cells for 2020 and Beyond. *Physica E: Low-Dimensional System and Nanostructures*, **14**, 65-70.

Green, M. A., 2003. Crystalline and Thin-Film Silicon Solar Cells: State of the Art and Future Potential. *Solar Energy*, **74**, 181-192.

Green, M. A., Emery, K., Hishikawa, Y., Warta, W. and Dunlop, E.D., 2015. Solar cell efficiency tables (version 47). *Progress in Photovoltaics: Research and Applications*, **24**, 3-11.

Griffini, G., Bella, F., Nisic, F., Dragonetti, C., Roberto, D., Levi, M., Bongiovanni, R., and Turri, S., 2015. Multifunctional Luminescent Down-Shifting Fluoropolymer Coatings: A Straightforward Strategy to Improve the UV-Light Harvesting Ability and Long-Term Outdoor Stability of Organic Dye-Sensitized Solar Cells. *Advanced Energy Materials*, **5**, 1401312.

Hägglund, C., Zäch, M., and Kasemo, B., 2008b. Enhanced Charge Carrier Generation in Dye Sensitized Solar Cells by Nanoparticle Plasmons. *Applied Physics Letters*, **92**, 013113.

Hägglund, C., Zäch, M., Petersson, G., and Kasemo, B., 2008a. Electromagnetic Coupling of Light into a Silicon Solar Cell by Nanodisk Plasmons. *Applied Physics Letters*, **92**, 053110.

Hebbink, G., 2002. Luminescent Materials Based on Lanthanide Ions. PhD thesis, *University of Twente*, the Netherlands.

Henglein, A., 1989. Small-Particle Research: Physicochemical Properties of Extremely Small Colloidal Metal and Semiconductor Particles. *Chemical Review*, **89**, 1861-1873.

Ho, W. J., Lee, Y. Y., Hu, C. H. and Sue, R. S., 2016. Plasmonics Modulation of Si Solar Cell with a Matrix Silver Nanoparticles Pattern Surrounded by Indium Nanoparticles. *Thin Solid Films*. http://dx.doi.org/10.1016/j.tsf.2016.05.019.

Hovel, H. J., Hodgson, R. T., and Woodall, J.M., 1979. The Effect of Fluorescent Wavelength Shifting on Solar Cell Spectral Response. *Solar Energy Materials*, **2**, 19-29.

Hsu, H. L., Juang, T.Y., Chen, C. P., Hsieh, C. M., Yang, C. C., Huang, C. L. and Jeng, R. J., 2015. Enhanced Efficiency of Organic and Perovskite Photovoltaics from Shape-Dependent Broadband Plasmonic Effects of Silver Nanoplates. *Solar Energy Materials and Solar Cells*, **140**, 224-231.

Hutter, E., and Fendler, J. H., 2004. Exploitation of Localized Surface Plasmon Resonance. *Advanced Materials*, **16**, 1685–1706.

Iranifam, M., 2016. Chemiluminescence Reactions Enhanced by Silver Nanoparticles and Silver Alloy Nanoparticles: Applications in Analytical Chemistry. *Trends in Analytical Chemistry*, **82**, 126-142.

Jang, E., Jun, S., Chung, Y., and Pu, L., 2004. Surface Treatment to Enhance the Quantum Efficiency of Semiconductor Nanocrystals. *The Journal of Physical Chemistry. B*, **108**, 4597-4600.

Karam, N. H., King, R. R., Cavicchi, B. T., Krut, D. D., Ermer, J. H., Cai, L., Haddad, M., Joslin, D. E., Takahashi, M., Eldredge, J. W., Nishikawa, W. T., Lillington, D. R., Keyes, B. M., and Ahrenkiel, R. K., 1999. Development and Characterization of High-Efficiency GaIn P/GaAs/Ge Dual- and Triple-Junction Solar Cells. *IEEE Transaction on Electronic Devices*, **46**, 2116- 2125.

Karatay, D. U., Salvador, M., Yao, K., Jen, A K. Y., and Ginger, D. S., 2014. Performance Limits of Plasmon-Enhanced Organic Photovoltaics. *Applied Physics Letters*, **105**, 033304.

Kawano, K., Hashimoto, N., and Nakata, R., 1997. Effects on Solar Cell Efficiency of Fluorescence of Rare-Earth Ions. *Materials Science Forum*, **239–241**, 311–314.

Kelly, K. L., Coronado, E., Zhao, L. L., and Schatz, G. C., 2003. The Optical Properties of Metal Nanoparticles: The Influence of Size, Shape, and Dielectric Environment. *The Journal of Physical Chemistry B*, **107**, 668–677.

Kennedy, M., Ahmed, H., Doran, J., Norton, B., Bosch- Jimenez, P., Della Pirriera, M., Torralba-Calleja, E., Tauste, D. G., Aubouy, L., Daren, S., Solomon-Tsvetkov, F., Galindo, S., Voz, C., and Puigdollers, J., 2015. Large Stokes Shift Downshifting Eu(III) Films as Efficiency Enhancing UV Blocking Layers for Dye Sensitized Solar Cells. *Physica Status Solidi*, **A 211**, 203-210.

Kennedy, M., McCormack, S. J., Doran, J., and Norton, B., 2009. Improving the Optical Efficiency and Concentration of a Single Plate Quantum Dot Solar Concentrator Using Near Infra-Red Emitting Quantum Dots. *Solar Energy*, **83**, 978-981.

Klampaftis, E., and Richards, B. S., 2011. Improvement in Multi-Crystalline Silicon Solar Cell Efficiency via Addition of Luminescent Material to EVA Encapsulation Layer. *Progress in Photovoltaics: Research and Applications*, **19**, 345–351.

Klampaftis, E., Ross, D., McIntosh, K. R., and Richards, B., 2009. Enhancing the Performance of Solar Cell via Luminescent Down-Shifting of the Incident Spectrum: A Review. *Solar Energy Materials & Solar Cells*, **93**, 1182-1194.

Klampaftis, E., Ross, D., Seyrling, S., Tiwari, A. N., and Richards, B. S., 2012. Increase in Short-Wavelength Response of Encapsulated CIGS Devices by Doping the Encapsulation Layer with Luminescent Material. *Solar Energy Material & Solar Cells*, **101**, 62–67.

Kreibig, U. and Vollmer, M. *Theoretical Considerations. In Optical Properties of Metal Clusters.* Springer Berlin Heidelberg, 1995, 13-201.

Kümmerlen, J., Leitner, A., Brunner, H., Aussenegg, F. R., and Wokaun, A., 1993. Enhanced dye Fluorescence over Silver Island Films: Analysis of the Distance Dependence. *Molecular physics*, **80**, 1031-1046.

Lakowicz, J, R., 2006a. Plasmonics in Biology and Plasmon-Controlled Fluorescence, *Plasmonics*, **1**, 5–33.

Lakowicz, J. R. Principles of Fluorescence Spectroscopy, *Springer, Third Edition*, New York, USA, 2006b.

Lakowicz, J. R., Geddes, C. D., Gryczynski, I., Malicka, J., Grynski, Z., Aslan, K., Lukomska, J., Matveeva, E., Zhang, J., Badugu, R., and Huang, J., 2004. Advance in Surface-Enhanced Fluorescence. *Journal of Fluorescence*, **14**, 425-441.

Lakowicz, J. R., Shen, Y., D'Auria,S., Malicka, J., Fang, J., Gryczynski, Z., and Gryczynski, I., 2002. Radiative Decay Engineering: Effects of Silver Island Films on Fluorescence Intensity, Lifetimes, and Resonance Energy Transfer. *Analytical Biochemistry***, 301,** 261-277.

Le Donne, A., Acciarri, M., Narducci, D., Marchionna, S., and Binetti. S., 2009. Encapsulating Eu^{3+} Complex Doped Layers to Improve Si-Based Solar Cell Efficiency. *Progress in Photovoltaics: Research and Applications*, **17**, 519-525.

Le Donne, A., Dilda, M., Crippa, M., Acciarri, M., and Binetti, S., 2011. Rare Earth Organic Complexes as Down-Shifters to Improve Si-Based Solar Cell Efficiency. *Optical Materials*, **33**, 1012–1014.

Lee, J. H., Park, J. H., Kim, J. S., Lee, D. Y., and Cho, K., 2009. High Efficiency Polymer Solar Cells with Wet Deposited Plasmonic Gold Nanodots. *Organic Electronics*, **10**, 416–420.

Leif, R. C., Vallarino, L. M., Becker, M. C., and Yang, S., 2006. Increasing the Luminescence of Lanthanide Complexes. *Cytometry A*, **69**, 767-778.

Levitt, J. A., and Weber, W. H., 1977. Materials for Luminescent Greenhouse Solar Collectors. *Applied Optics*, **16**, 2684–2689.

Li, H., Kang, J., Yang, J. and Wu, B., 2016. Fabrication of $Au_{nanoparticle}$ @ $mSiO_2$ @ Y_2O_3: Eu Nanocomposites with Enhanced Fluorescence. *Journal of Alloys and Compounds*, **673**, 283-288.

Li, X. F., Lau, K.T., An, Y., Yin, Y. S., and Wong, T. T., 2008. Luminescent and Mechanical Properties of the Epoxy Composites doped with Europium Complex. *Materials Letters*, **62**, 4434-4436.

Lim, S. H., Mar, W., Matheu, P., Derkacs, D., and Yu, E. T., 2007. Photocurrent Spectroscopy of Optical Absorption Enhancement via Scattering from Surface Plasmon Polaritons in Gold Nanoparticles. *Applied Physics Letters*, **101**, 104309.

Link, S., and El-Sayed, M. A., 2000. Shape and Size Dependence of Radiative, Non-radiative and Photothermal Properties of Gold Nanocrystals. *International Reviews in Physical Chemistry*, **19**, 409-453.

Liu, X. H., Hou, L. X., Wang, J. F., Liu, B., Yu, Z. S., Ma, L. Q., Yang, S. P. and Fu, G. S., 2014. Plasmonic-Enhanced Polymer Solar Cells with High Efficiency by Addition of Silver Nanoparticles of Different Sizes in Different Layers. *Solar Energy*, **110**, 627-635.

Louwen, A., Van Sark, W., Schropp, R. and Faaij, A., 2016. A cost Roadmap for Silicon Heterojunction Solar Cells. *Solar Energy Materials and Solar Cells*, **147**, 295-314.

Ma, G. F., Xie, H., Cheng, P. P., Li, Y. Q., and Tang, J. X., 2013. Performance Enhancement of Polymer Solar Cells with Luminescent Down-Shifting Sensitizer. *Applied Physics Letter*, **103**, 043302.

Maier, S. A. *Plasmonics: Fundamentals and Applications*. Springer, New York, USA, 2007; Chapter 8, p.141.

Marchionna, S., Meinardi, F., Acciarri, M., Binetti, S., Papagni, A., Pizzini, S., Malatesta, V., and Tubino, R., 2006. Photovoltaic Quantum Efficiency Enhancement by Light Harvesting of Organo-Lanthanide Complexes. *Journal of Luminescence*, **118**, 325–329.

Maruyama, T., and Kitamura, R., 2001. Transformation of the Wavelength of the Light Incident upon CdS/CdTe Solar Cells. *Solar Energy Material & Solar Cells*, **69**, 61-68.

Maruyama, T., Enomoto, A., and Shirasawa, K., 2000. Solar Cell Module Colored with Fluorescent Plate. *Solar Energy Materials & Solar Cells*, **64**, 269–278.

McIntosh, K. R., Lau, G., Cotsell, J. N., Hanton, K., and Batzner, D. L., 2009. Increase in External Quantum Efficiency of Encapsulated Silicon Solar Cells from a Luminescent Down-Shifting Layer. *Progress in Photovoltaics: Research and Application*, **17**, 191-197.

Mcnay, G., Eustace, D., Smith, W. E., Faulas, K., and Graham, D., 2011. Surface-Enhanced Raman Scattering (SERS) and Surface-Enhanced Resonance Raman Scattering (SERRS): A Review of Applications. *Applied Spectroscopy*, **65**, 825-837**.**

Mićić, O. I., Cheong, H. M., Fu, H., Zunger , A., Sprague , J. R., Mascarenhas, A., and Nozik, A. J., 1997. Size-Dependent Raman Study of InP Quantum Dots. *The Journal of Physical Chemistry B*, **101**, 4909-4912.

Mie, G., 1908. Contribution to Optics of Turbid Media, Especially Colloidal Metal Solutions. *Annals Physics*, **25**, 378-445.

Morfa, A. J., Rowlen, K. L., Reilly III, T. H., Romero, M. J., and van de Lagemaat, J., 2008. Plasmon-Enhanced Solar Energy Conversion in Organic Bulk Heterojunction Photovoltaics. *Applied Physics Letters*, **92**, 013504.

Moudam, O., Rowan, B. C., Alamiry, M., Richardson, P., Richards, B. S., Jones, A. C., and Robertson, N., 2009. Europium Complexes with High Total Photoluminescence Quantum Yields in Solution and in PMMA. *Chemical Communications*, **43**, 6649-6651.

Musken, O. L., Giannini, V., Sánchez, J. A., and Rivas, J. G., 2007. Strong Enhancement of the Radiative Decay Rate of Emitter by Single Plasmonic Nanoantennas. *Nano Letters*, **7**, 2871-2875.

Nakayama, K., Tanabe, K., and Atwater, H. A., 2008. Plasmonic Nanoparticle Enhanced Light Absorption in GaAs Solar Cells. *Applied Physics Letters*, **93**, 121904.

Noguez, C., 2007. Surface Plasmons on Metal Nanoparticles: The Influence of Shape and Physical Environment. *Journal of Physics Chemistry C*, **111**, 3806-3819.

Novotny, L., 1996. Single Molecule Fluorescence in Inhomogeneous Environments. *Applied Phys*ics *Letters*, **69**, 3806-3808.

NREL, 2016. National Renewable Energy Laboratory Renewable Energy, US Department of Energy, *Available Online* at http://www.nrel.gov/ncpv/ and http://www.nrel.gov/ncpv/images/efficiency_chart.jpg. Last accessed 12/8/2016.

Pala, R. A., White, J., Barnard, E., Liu, J., and Brongersma, M. L., 2009. Design of Plasmonic Thin-Film Solar Cells with Broadband Absorption Enhancements. *Advanced Materials*, **21**, 3504–3509.

Peumans, P., Yakimov, S., and Forrest, S. R., 2003. Small Molecular Weight Organic Thin-Film Photodetectors and Solar Cells. *Journal of Applied Physics*, **93**, 3693- 3723.

Pickett, N. L., and O'Brien, P., 2001. Syntheses of Semiconductor Nanoparticles Using Single-Molecular Precursors. *The Chemical Record*, **1**, 467-479.

Pillai, S., Catchpole, K. R., Trupke, T., and Green, M. A., 2007. Surface plasmon enhanced silicon solar cells. *Journal of Applied Physics*, **101**, 093105.

Pillai, S., Catchpole, K. R., Trupke, T., Zhang, G., Zhao, J., and Green, M. A., 2006 Enhanced Emission From Si-Based Light-Emitting Diodes Using Surface Plasmons. *Applied Physics Letters*, **88**, 161102.

PlasmaChem GmbH Quantum Dots Product Information. *Available Online* at http://www.plasmachem.com/. Last accessed 12/8/2016.

Prasad, P. N. *Nanophotonics*. John Wiley & Sons, Inc., Hoboken, New Jersey, USA, 2004; Chapter 5, p.129.

Ramanathan, K., Keane, J., and Noufi, R., 2005. Properties of High-Efficiency CIGS Thin-Film Solar Cells *In the proceeding of the 31st IEEE Photovoltaics Specialists Conference and Exhibition* Lake Buena Vista, Florida.

Razykov, T. M., Ferekides, C. S., Morel, D., Stefanakos, E., Ullal, H. S., and Upadhyaya, H. M., 2011. Solar Photovoltaic Electricity: Current Status and Future Prospects. *Solar Energy*, **85**, 1580–1608.

Reisfeld, R., 1983. Future Technological Applications of Rare Earth Doped Materials. *Less Common Metals*, **93**, 243–251.

Reisfeld, R., Eyal, M., and Brusilovsky, D., 1988. Luminescence Enhancement of Rhodamine 6G in Sol-Gel Films Containing Silver Aggregates. *Chemical Physics Letters*, **153**, 210-214.

Reisfeld, R., Saraidarov, T., and Levchenko, V., 2009. Strong Emitting Sol–Gel Materials Based on Interaction of Luminescence Dyes and Lanthanide Complexes with Silver Nanoparticles. *Journal of Sol-Gel Science and Technology*, **50**, 194–200.

Reisfeld. R., 2010. New Developments in Luminescence for Solar Energy Utilization. *Optical Materials*, **32**, 850–856.

Ren, Z., Li, X., Guo, J., Wang, R., Wu, Y., Zhang, M., Li, C., Han, Q., Dong, J. and Zheng, H., 2015. Solution-Based Metal Enhanced Fluorescence with Gold and Gold/Silver Core–Shell Nanorods. *Optics Communications*, **357**, 156-160.

Ross, D., Alonso-Álvarez, D., Klampaftis, E., Fritsche, J., Bauer, M., Debije, M. G., Fifield, R. M., and Richards, B. S., 2014. The Impact of Luminescent Down Shifting on the Performance of CdTe Photovoltaics: Impact of the Module Vintage. *IEEE Journal of Photovoltaic*, **4**, 457-464.

Ross, D., Klampaftis, E., Fritsche, J., Bauer, M., and Richards, B. S., 2012. Increased Short-Circuit Current Density of Production Line CdTe Mini-Module through Luminescent Down-Shifting. *Solar Energy Materials & Solar Cells*, **103**, 11-16.

Rothemund, R., Kreuzer, S., Umundum, T., Meinhardt, G., Fromherz, T., and Jantsch, W., 2011. External Quantum Efficiency Analysis of Si Solar Cells with II-VI Nanocrystal Luminescent Down-Shifting Layers. *Energy Procedia*, **10**, 83-87.

Rowan, B. C., Wilson, L. R., and B.S. Richards, B. S., 2008. Advanced Material Concepts for Luminescent Solar Concentrators. *IEEE J. Selected Topics in Quantum Electronics*, **14**, 1312-1322.

Sadeghimakki, B., and Sivoththaman, S., 2010. Uniform Embedment of CdSe/ZnS Quantum Dot Arrays in Thin Oxide Layers for Luminescence Down Shifting in PV Devices. *In Proceedings of 35th IEEE Photovoltaic Specialists Conference (PVSC)*, 002955-002959.

Sardar, D. K., Nash, K. L., Yow, R. M., and Gruber. J. B., 2006. Absorption Intensities and Emission Cross Sections of Tb^{3+} ($4f^8$) in $TbAlO_3$. *Journal of Applied Physics*, **100**, 083108.

Schüler, A., Python, M., Valle del Olmo, M., and de Chambrier, E., 2007. Quantum Dot Containing Nanocomposite Thin Films for Photoluminescent Solar Concentrators. *Solar Energy*, **81**, 1159–1165.

Shan, F., Zhang, T., and Zhu, S. Q., 2014. Effects of Ag Nanocubes with Different Corner Shape on the Absorption Enhancement in Organic Solar Cells. *Journal of Nanomaterials*, **2014**, 1-8.

Shavaleev, N. M., Scopelliti, R., Gumy, F., and Bünzli, J.-C., 2008. Visible-Light Excitation of Infrared Lanthanide Luminescence via Intra-Ligand Charge-Transfer State in 1, 3-Diketonates Containing Push-Pull Chromophores. *European Journal of Inorganic Chemistry*, **2008**, 1523-1529.

Shetty, K. D., Boreland, M. B., Shanmugam, V., Cunnusamy, J., Wu, C-K., Iggo, S., and Antoniadis, H., 2013. Lightly Doped Emitters for High Efficiency Silicon Wafer Solar Cells. *Energy Procedia*, **33**, 70 – 75.

Shirasaki, Y., Supran, G.J., Bawendi, M.G. and Bulović, V., 2013. Emergence of colloidal quantum-dot light-emitting technologies. *Nature Photonics*, **7(1)**, pp.13-23.

Sholin, V., Olson, J. D., and Carter, S. A., 2007. Semiconducting Polymer and Quantum Dots in Luminescent Solar Concentrators for Solar Energy Harvesting. *Journal of Applied Physics*, **101**, 123114.

Shunmugam, R., and Tew, G. T., 2005. Unique Emission from Polymer Based Lanthanide Alloys. *Journal of the American Chemical Society*, **127**, 13567-13572.

Slooff, L. H., Kinderman, R., Burgers, A. R., Büchtemann, A., Danz, R., Meyer, T. B., Chatten, A. J., Farrell, D. Barnham, K. W J., and van Roosmalen, J. A. M., 2006. The Luminescent Concentrator Illuminated. *In Proceedings of Society of Photographic Instrumentation Engineers (SPIE)* **6197**, 61970K.

Slooff, L. H., Kinderman, R., Burgers, A. R., van Roosmalen, J. A. M., Büchtemann, A., Danz, R., Schleusener, M., Chatten, A. J., Farrell, D., and Barnham, K. W. J., 2005. The Luminescent Solar Concentrator: A Bright Idea for Spectrum Conversion? *In Proceedings of the 20th European Photovoltaic Solar Energy Conference and Exhibition*, Barcelona, Spain, 413-416.

Slooff, L. H., van Blaaderen, A., Polman, A., Hebbink, G. A., Klink, S. I., van Veggel, F. C., Reinhoudt, D. N., and Hofstraat, J. W., 2002. Rare-Earth Doped Polymers for Planar Optical Amplifiers. *Journal of Applied Physics Reviews*, **91**, 3955-3980.

Stenzel, O., Stendal, A., Voigtsberger, K., and von Borczyskowski, C., 1995. Enhancement of the Photovoltaic Conversion Efficiency of Copper Phthalocyanine Thin Film Devices by Incorporation of Metal Clusters. *Solar Energy Materials and Solar Cells*, **37**, 337-348.

Stranik, O., 2007. Plasmonic Enhancement of Fluorescence for Biomedical Diagnostics. PhD thesis, Dublin City University, Ireland.

Stranik, O., McEvoy, H. M., McDonagh, C., and MacCraith, B. D., 2005, Plasmonic Enhancement of Fluorescence for Sensor Applications. *Sensors and Actuators B*. **107**, 148-153.

Strohhöfer, C., and Polman, A., 2002. Silver as a Sensitizer for Erbium. *Applied Physics Letters*, **81**, 1414–1416.

Strümpel, C., McCann, M., Beaucarne, G., Arkhipov, V., Slaoui, A., Švrček, V., del Cañizo, C., and Tobias, I., 2007. Modifying the Solar Spectrum to Enhance Silicon Solar Cell Efficiency- An Overview of Available Materials. *Solar Energy Materials & Solar Cells*, **91**, 238-249.

Stuart, H. R., and Hall, D. G., 1998. Island Size Effects in Nanoparticle-Enhanced Photodetectors. *Applied Physics Letters*, **73**, 3815–3817.

SunShot Vision Study, 2012, US Department of Energy, *Available Online* at *http://www.nrel.gov/docs/fy12osti/47927.pdf*. Last accessed 12/08/2016.

Švrček, V., Slaoui, A., and Muller, J.-C., 2004. Silicon Nanocrystals as Light Converter for Solar Cells. *Thin Solid Films*, **451–452**, 384–388.

Swift, P. D., and Smith, G. B., 2003. Color Considerations in Fluorescent Solar Collector Stacks. *Applied Optics*, **42**, 5112-5117.

Tam, F., Goodrich, G. P., Johnson, B. R., and Halas, N. J., 2007. Plasmonic Enhancement of Molecular Fluorescence. *Nano Letters*, **7**, 496-501.

Tanaka, N., Barashkov, N., Heath, J., and Sisk, W. N., 2006. Photodegradation of Polymer-Dispersed Perylene Di-Imide Dyes. *Applied Optics*, **45**, 3846-3850.

Temple, T. L., Mahanama, G. D. K., Reehal, H. S., and Bagnall, D. M., 2009. Influence of Localized Surface Plasmon Excitation in Silver Nanoparticles on the Performance of Silicon Solar Cells. *Solar Energy Materials & Solar Cells*, **93**, 1978–1985.

Tsao, J., Lewis, N. and Crabtree, G., 2006. Solar FAQs. *US department of Energy*.

Van der Ende, B. M., Aarts, L., and Meijerink, A., 2009. Lanthanide Ions as Spectral Converters for Solar Cells. *Physical Chemistry Chemical Physics*, **11**, 1108-1195.

Van Deun, R., Fias, P., Nockemann, P., Van Hecke, K., Van Meervelt, L., and Binnemans, K., 2006. Visible-Light-Sensitizes Near-Infrared Luminescence from Rare-Earth Complexes of the 9-Hydroxyphenalen-1-One Ligand. *Inorganic Chemistry*, **45**, 10416-10418.

Van Sark, W. G. J. H. M., 2006. Optimization of the Performance of Solar Cells with Spectral Downshifting Converts. *In the proceeding* of *21st European Photovoltaic Solar Energy Conference*, Dresden, Germany, 155-159.

Van Sark, W. G. J. H. M., Meijerink, A., Schropp, R. E. I., Van Roosmalen, J. A. M., and Lysen, E. H., 2004. Modeling Improvement of Spectral Response of Solar Cells by Deployment of Spectral Converters Containing Semiconductor Nanocrystals. *Semiconductors*, **38**, 962–969.

Wang, R., Wang, X., and Zhou, Z., 2012. Photocurrent Enhancement in Plasmonic Solar Cells Attached to Luminescent Solar Concentrators. *In the Proceeding of SPIE*, **8468**, 84680B-1.

Wang, S. Y., Borca-Tasciuc, D. A., and Kaminski, D. A., 2011b. Spectral Coupling of Fluorescent Solar Concentrators to Plasmonic Solar Cells. *Journal of Applied Physics*, **109**, 074910.

Wang, X., Wang, T., Tian, X., Wang, L., Wu, W., Luo, Y., and Zhang, Q., 2011a. Europium Complex Doped Luminescent Solar Concentrators with Extended Absorption Range from UV to Visible Region. *Solar Energy*, **85**, 2179-2184.

Wang, Y., 2009. Recent Research Progress on Polymer Electrolytes for Dye-Sensitized Solar Cells. *Solar Energy Materials & Solar Cells*, **93**, 1167-1175.

Weber, W. H., and Lambe, J., 1976. Luminescent Collector for Solar Radiation. *Applied Optics*, **15**, 2299-2300.

Werts, M. H., Jukes, R. T., and Verhoeven, J. W., 2002a. The Emission Spectrum and the Radiative Lifetime of Eu^{3+} in Luminescent Lanthanide Complexes. *Physical Chemistry Chemical Physics*, **4**, 1542–1548.

Werts, M. H., Verhoeven, J. W., and Hofstraat, J. W., 2002b. Efficient Visible Light Sensitisation of Water-Soluble Near-Infrared Luminescent Lanthanide Complexes. *Journal of the Chemical Society Perkin Transection*, **2**, 433–439.

Westphalen, M., Kreibig, U., Rostalski, J., Lüth, H., Meissner, D., 2000. Metal Cluster Enhanced Organic Solar Cells. *Solar Energy Materials & Solar Cells*, **61**, 97-105.

Wilson, H. R., 1987. Fluorescent Dyes Interacting with Small Silver Particles; A System Extending the Spectral Range of Fluorescent Solar Concentrators. *Solar Energy Materials*, **16**, 223-234.

Wilson, L. R., 2010. Luminescent Solar Concentrators: A Study of Optical Properties, Re-absorption and Device Optimisation. PhD Thesis, Heriot-Watt University, UK.

Wohnhaas, C., Friedemann, K., Busko, D., Landfester, K., Baluschev, S., Crespy, D., Turshatov, A., 2013. All Organic Nanofibers As Ultralight Versatile Support for Triplet–Triplet Annihilation Upconversion. *American Chemical Society Macro Letters* **2,** 446–450.

Wokaun, A., Lutz, H. P., King, A. P., Wild, U. P., and Ernst, R. R., 1983. Energy Transfer in Surface Enhanced Luminescence. *The Journal of Chemical Physics*, **79**, 509.

Wong, K.-L., Souici, A., De Waele, V., Mostafavi, M., Metzger, T. H., and Mintova, S., 2010. Subnanometer CdS Clusters Self-Confined in MFI-Type Zeolite Nanoparticles and Thin Films. *Langmuir*, **26**, 4459-4464.

Wu, C., Zhou, X. and Wei, J., 2015. Localized Surface Plasmon Resonance of Silver Nanotriangles Synthesized by a Versatile Solution Reaction. *Nanoscale research letters*, **10**, DOI 10.1186/s11671-015-1058-1.

Wu, M., Lakowicz, J. R., and Geddes, C. D., 2005. Enhanced Lanthanide Luminescence Using Silver Nanostructures: Opportunities for a New Class of Probes with Exceptional Spectral Characteristics. *Journal of Fluorescence*, **15**, 53-59.

Xiao, M., and Selvin, P. R., 2001. Quantum Yields of Luminescent Lanthanide Chelates and Far-Red Dyes Measured by Resonance Energy Transfer. *Journal of the American Chemical Society*, **123**, 7067-7073.

Xiaodong, P., Qing, L., Dongsheng, L., and Deren, Y., 2011. Spin-Coating Silicon-Quantum-Dot Ink to Improve Solar Cell Efficiency. *Solar Energy Materials & Solar Cells*, **95**, 2941-2945.

Xu, L., Ma, Y. F., Tang, K. Z., Tang, Y., Liu, W. S., and Tan, M. Y., 2008. Preparation, Characterization and Photophysical Properties of Highly Luminescent Terbium Complexes Incorporated into SiO2/Polymer Hybrid Material. *Journal of Fluorescence*, **18**, 685-693.

Xu, S., Zhang, J., Song, X., Dai, Z., and Sun, B., 2007. Luminescent CdTe/CdS Core-Shell and CdTe/CdS/ZnS Multi-Layer Quantum Dots: Synthesis and Investigations for Bioapplication. *In Proceeding of Society of Photographic Instrumentation Engineers Conference (SPIE)*, **6831**, 68310U-1.

Xu, X., Kyaw, A.K.K., Peng, B., Zhao, D., Wong, T.K., Xiong, Q., Sun, X.W. and Heeger, A.J., 2013. A Plasmonically Enhanced Polymer Solar Cell with Gold–Silica Core–Shell Nanorods. *Organic Electronics*, **14**, 2360-2368.

Yakimov, A., and Forrest, S. R., 2002. High Photovoltage Multiple-Heterojunction Organic Solar Cells Incorporating Interfacial Metallic Nanoclusters. *Applied Physics Letters*, **80**, 1667-1669.

Yanagida, S., Hasegawa, Y., and Wada, Y., 2000. Remarkable Luminescence of Novel Nd(III) Complexes with Low-Vibrational Hexafluoroacetylacetone and DMSO-d_6 Molecules. *Journal of Luminescence*, **87-89**, 995-998.

Yang, Y., Lin, X., Qing, J., Zhong, Z., Ou, J., Hu, C., Chen, X., Zhou, X., and Chen, Y., 2014. Enhancement of Short-Circuit Current Density in Polymer Bulk Heterojunction Solar Cells Comprising Plasmonic Silver Nanowires. *Applied Physics Letters*, **104**, 123302.

Yu, J., Shao, W., Zhou, Y., Wang, H., Liu, X., and Xu, X., 2013. Nano Ag-Enhanced Energy Conversion Efficiency in Standard Commercial pc-Si Solar Cells and Numerical Simulations with Finite Difference Time Domain Method. *Applied Physics Letters*, **103**, 203904.

Zweibel, K., 2005. The Terawatt Challenge for Thin Film PV**,** National Renewable Energy Laboratory (NREL) Technical Report, *Available Online* at http://www.nrel.gov/docs/fy05osti/38350.pdf **,** 1-49. Last accessed 12/08/2016.